HHS Public Access

Author manuscript

Nature. Author manuscript; available in PMC 2019 November 15.

Published in final edited form as:

Nature. 2019 June ; 570(7759): 112–116. doi:10.1038/s41586-019-1215-2.

Targeting the CBM complex causes Treg cells to prime tumors for immune checkpoint therapy

Mauro Di Pilato[1,2,*], **Edward Y. Kim**[1,2,*], **Bruno L. Cadilha**[1], **Jasper N. Pruessmann**[1,2], **Mazen N. Nasrallah**[1,2], **Davide Seruggia**[2,3], **Shariq M. Usmani**[1,2], **Sandra Misale**[2,4], **Valentina Zappulli**[5], **Esteban Carrizosa**[1,2], **Vinidhra Mani**[1,2], **Matteo Ligorio**[2,4], **Ross D. Warner**[1], **Benjamin D. Medoff**[1,2], **Francesco Marangoni**[1,2], **Alexandra-Chloe Villani**[1,2], **Thorsten R. Mempel**[1,2]

[1]Center for Immunology and Inflammatory Diseases, Massachusetts General Hospital, Boston, MA

[2]Harvard Medical School, Boston, MA

[3]Division of Hematology/Oncology, Boston Children's Hospital, Boston, MA

[4]Center for Cancer Research, Massachusetts General Hospital, Boston, MA

[5]Department of Comparative Biomedicine and Food Science, University of Padua, Italy

Abstract

Solid tumors are infiltrated by effector T cells (Teff) with the potential to control or reject them, as well as by regulatory T cells (Treg) that restrict the function of Teff and thereby promote tumor growth.[1] The anti-tumor activity of Teff can be therapeutically unleashed and is now being exploited for the treatment of some forms of human cancer. However, weak tumor-associated inflammatory responses and the immune-suppressive function of Treg remain major hurdles to broader effectiveness of tumor immunotherapy.[2] Here we show that upon disruption of the CARMA1-BCL10-MALT1 (CBM) signalosome complex, the majority of tumor-infiltrating Treg produce IFN-γ, followed by stunted tumor growth. Remarkably, genetic deletion of both or even just one allele of *Carma1* in only a fraction of Treg, which avoided systemic autoimmunity, was sufficient to produce this anti-tumor effect, showing that not mere loss of suppressive function, but

¶Correspondence should be addressed to: T.R.M. (tmempel@mgh.harvard.edu) or M.D.P. (mdipilato@mgh.harvard.edu).
*Authors contributed equally to this work

Author contributions. M.D.P. initiated, designed, performed and analyzed the experiments, and wrote the paper. E.Y.K. initiated the project, designed and performed experiments, V.Z. performed histological analyses, S.M.U. performed autoantibody assays, V.M. and F.M performed Treg analyses in lung and skin. F.M performed in vitro Treg suppression assay. E.C. generated tumor cell lines. M.N. and A.C.V. performed RNA-Seq analyses, B.D.M. provided genetic mouse models, D.S. designed and performed RT-qPCR assay, B.C., S.M., J.N.P., R.W., M.L. performed tumor growth studies and survival studies, T.R.M. conceived the study, supervised the project, designed experiments, and wrote the manuscript.

Data availability

All data sets generated during the current study are available from the corresponding authors upon reasonable request. RNA-sequencing data have been deposited at the Gene Expression Omnibus (GEO) under accession number GSE129480.

M.D.P. and T.R.M. have filed a patent application related to the use of MALT1 inhibitors. T.R.M. is a co-founder of Monopteros Therapeutics. All other authors declare no competing interests. Readers are welcome to comment on the online version of the paper.

gain of effector activity by Treg initiates tumor control. Treg-production of IFN-γ was accompanied by macrophage activation and up-regulation of MHC-I on tumor cells. However, tumor cells also up-regulated expression of PD-L1, indicating activation of adaptive immune resistance.[3] Consequently, PD-1 blockade concomitant with CARMA1-deletion caused rejection of tumors that otherwise do not respond to anti-PD-1 monotherapy. This effect was reproduced by pharmacological inhibition of the CBM protein MALT1. Our results demonstrate that partial disruption of the CBM complex and induction of IFN-γ-secretion in the preferentially self-reactive Treg pool does not cause systemic autoimmunity but is sufficient to prime the tumor environment for successful immune checkpoint therapy.

Keywords

Tumor microenvironment; Tumor inflammation; Adaptive Immune Resistance; Immune Checkpoint Therapy; PD-1; Regulatory T cell stability; CARMA1/CARD11; MALT1 Paracaspase

Local exposure of tumor-infiltrating Treg to their cognate antigens sustains their tumor-promoting immunosuppressive functions.[4] We therefore explored which T-cell receptor (TCR)-dependent signaling pathways could be targeted to disable tumor-reactive Treg. The scaffold protein CARMA1/Card11 nucleates assembly of the CBM complex in T cells in response to TCR-dependent PKCθ activity and promotes several functions, including activation of the AP-1, mTOR, and classical NF-κB pathways, as well as mRNA stabilization.[5] Constitutive genetic deletion of CARMA1, BCL10, or MALT1 abrogates thymic Treg development,[6–10] but their role in mature Treg is unknown.

When we conditionally deleted either one or both alleles of *Carma1* in mature Treg by crossing Foxp3$^{YFP\text{-}Cre}$ to CARMA1$^{flox/flox}$ mice (hereafter called F^{Cre} x C1$^{f/+}$ or x C1$^{f/f}$), CARMA1 protein was proportionally reduced in CD4^{+} Foxp3^{+} Treg from lymph nodes (LNs) (Ext Data Fig. 1a). F^{Cre} x C1$^{f/f}$, but neither F^{Cre} x C1$^{f/+}$ or C1$^{+/+}$ control mice, stopped thriving at 17 days and their majority died before 4 weeks of age following a T_H1-dominated multiorgan inflammatory disease characterized by splenomegaly, lymphadenopathy, effector differentiation and inflammatory cytokine-secretion by conventional T cells (Tconv), production of autoreactive IgG, and activation of the myeloid compartment. (Fig. 1a, Ext. Data Figs. 1b–f and 2a–f). Hence, CARMA1 is essential for Treg to maintain immune homeostasis, but expression reduced to 50% is tolerated.

Absolute numbers of Treg were increased in LNs of F^{Cre} x C1$^{f/f}$ mice, concomitant with an increase in overall LN cellularity (Ext. Data Fig. 2g–h). However, their overall frequency among CD4^{+} T cells did not vary with CARMA1 expression, while the proportion of CD44^{hi} CD62L^{-} effector Treg ('eTreg') was strongly reduced in its absence (Fig. 1b). Strikingly, CARMA1-deficient Treg, while retaining Foxp3 expression, almost uniformly secreted IFNγ and, at lower frequencies, IL-4, IL-17, and TNF (Fig. 1c). Although nearly all CARMA1-deficient Treg secreted the T_H1-cytokine IFNγ, much fewer, and only eTreg, expressed the T_H1 lineage-defining transcription factor T-bet along with RORγt and, to a lesser degree, GATA-3 (Fig. 1d and Ext. Data Fig. 2i–j). Hence, complete, but not partial deletion of CARMA in Treg profoundly dysregulates their cytokine expression that, in the case of IFNγ, is dissociated from expression of T-bet, and may contribute to inflammatory

disease pathogenesis. Indeed, F^{Cre} x $C1^{f/f}$ mice died more rapidly than Treg-deficient *scurfy* mice, but their lifespan was similar when IFNγ was neutralized (Fig. 1e). Thus, under inflammatory conditions, CARMA1-deficient Treg convert from an immunoregulatory into an IFNγ-secreting pathogenic cell type.

In heterozygous female $F^{Cre/+}$ x $C1^{f/f}$ mice, random X-inactivation causes the YFP-Cre fusion protein to be expressed and CARMA1 to be deleted in only half of Treg, while the other half maintains immune homeostasis (Ext. Data Fig. 3a–c). Under such non-inflammatory conditions CARMA1-deficient Treg did not secrete effector cytokines (Fig. 1f). However, in competition with CARMA1-sufficient Treg for niche space, we observed a proportional decline specifically in the frequency of eTreg (but not of cTreg) that lacked one or both alleles of *Carma1* (Fig. 1g and Ext. Data Fig. 3e). The remaining YFP^+ eTreg also expressed less Foxp3 and markers of eTreg differentiation (Fig. 1h). They expressed more pro-apoptotic Bim, but also more anti-apoptotic Bcl-2, likely reflecting impaired eTreg differentiation, since control eTreg strongly downregulated both Bcl-2 and Bim relative to cTreg (Ext. Data Fig. 3d–h). In vitro suppressive function of CARMA1-deficient Treg was reduced, but not abrogated (Ext. Data Fig. 4a–b), while they failed to persist and did not suppress lymphopenia-induced expansion of Teff upon transfer into Rag-deficient hosts (Ext. Data Fig. 4c). Failure to persist in vivo did not appear to result from accelerated apoptosis, since the previously described high apoptotic rate of eTreg[11] was not further enhanced in the absence of CARMA1 (Ext. Data Fig. 4d). Lack of CARMA1 also did not lead to an increase in the formation of $Foxp3^-$ exTreg (Ext. Data Fig. 4e).

Based on global gene expression analyses, CARMA1-deficient eTreg were equally dissimilar to control eTreg as they were to control cTreg, while CARMA1-deficient cTreg were only moderately dissimilar to control cTreg (Fig. 1i). In the latter, only 96 genes were differentially expressed, compared to 344 genes in eTreg (Ext. Data Fig. 5a, and Table S1). Based on differences between control cTreg and eTreg we defined an ‘eTreg signature’, which largely overlapped with a previously reported gene set.[12,15] When examining these 689 genes, hemizygous *Carma1*-deletion had only moderate impact, while homozygous deletion induced major changes specifically in the eTreg gene expression program (Fig. 1j and Ext. Data Fig. 5b). Minor changes in expression of Bcl2 family apoptotic regulator genes occurred during eTreg differentiation, but CARMA1-deficient eTreg did not deviate from this pattern apart from less pronounced down-regulation of Bcl2 and Bim, confirming our observations on protein expression (Ext. Data Fig. 6). Thus, loss and already a decrease in CARMA1 expression impairs eTreg differentiation and persistence, but does not induce them to become pathogenic or convert to exTreg under non-inflammatory conditions. However, in the context of incipient inflammation trigged by global loss of Treg suppressive function, CARMA1-deficient Treg secrete IFNγ, which further accelerates inflammatory disease.

Failed thymic Treg development in absence of CARMA1 results from disabled NF-κB signaling and is restored through expression of IKK2ca, a constitutively active form of IKK2/β.[12] Furthermore, NF-kB proteins c-Rel and p65/RelA have important roles in Treg function,[13–15] suggesting that failed NF-kB activation may primarily account for the effects of CARMA1-deletion in Treg. However, expression of IKK2ca in Treg neither prolonged the

lifespan of F^{Cre} x $C1^{f/f}$ mice, nor reduced Tconv effector differentiation (Ext. Data Fig. 7a–b). Restoring NF-κB activation did not restore eTreg differentiation either, and did not limit secretion of IFNγ, but only of TNF (Ext. Data Fig. 7c–d). Therefore, although NF-kB activation is evidently essential,[15,16] additional CBM-complex effector functions are similarly critical to maintaining Treg function. The relevance of these additional functions will need to be investigated, but an initial examination of CARMA1-deficient Treg from healthy $F^{Cre/+}$ x $C1^{f/f}$ mice already revealed decreased expression and TCR-induced phosphorylation of the AP-1 family protein c-Jun, as well as changes to Foxo1-phosphorylation, possibly reflecting CARMA1- and TBK1-driven regulation of Akt activity[17] (Ext. Data Fig. 7e–f).

Considering the pro-inflammatory potential of CARMA1-deficient Treg, we examined their tumor response. Subcutaneous implantation of the poorly immunogenic $BRAF^{V600E}$ x $PTEN^{null}$ melanoma D4M.3A (Ref.[18]) into female $F^{Cre/+}$ x $C1^{f/f}$ hosts amplified the effects of CARMA1-deficiency on Treg, since the frequency not only of eTreg, but even of total Treg was reduced in tumors and tumor-draining LNs (tdLNs) as a function of decreasing CARMA1-expression, accompanied also by more pronounced reduction in Foxp3 expression (Ext. Data Fig. 8a–d). Interestingly, we noted growth deceleration of D4M.3A melanoma, and also of MC38 colon carcinoma, when half of Treg lacked either one or both alleles of *Carma1* (Fig. 2a and Ext. Data Fig. 8e). Since a mere loss of function in only half of Treg is not predicted to cause loss of tumor tolerance,[19] this suggested active Treg-mediated anti-tumor activity. Indeed, a large fraction of either completely or even just partially CARMA1-deficient Treg secreted both TNF and IFNγ in situ, while these effector cytokines were undetectable in tumor-infiltrating $CD4^+$ and $CD8^+$ Tconv (Fig. 2b–c). Importantly, no increase in Treg cytokine secretion was observed in tdLNs or in non-lymphoid tissues, such as skin or lung (Fig. 2d and Ext. Data Fig. 8f–g). IFNγ-expression in tumor tissue correlated with down-regulation, but not loss of Foxp3 in both partially and fully CARMA1-deficient Treg (Ext. Data Fig. 8h). Notably, destabilization of control Treg by IFNγ-producing Treg, as described in other settings,[20] did not occur since no increase in cytokine expression was detectable in YFP^- CARMA1-sufficient Treg in the same tumors (**not shown**). Neutralization of IFNγ fully restored tumor growth in $F^{Cre/+}$ x $C1^{f/f}$ mice (Ext. Data Fig. 8i), suggesting an critical role for this cytokine in Treg-mediated anti-tumor immunity. However, IFNγ may also derive from other cellular sources following Treg destabilization. To specifically test the role of Treg-produced IFNγ we transferred Treg with reduced CARMA1 expression into tumor-bearing C57BL/6 or $Ifng^{-/-}$ mice. In both hosts Treg stunted tumor growth similarly, but not when IFNγ was neutralized, indicating that Treg-derived IFNγ is both necessary and sufficient for anti-tumor effects (Fig. 2e–f and Ext. Data Fig. 8j–m). Therefore, while neither partially nor fully CARMA1-deficient Treg cause inflammation in healthy mice, they are selectively destabilized in tumor tissue and secrete IFNγ to decelerate tumor growth.

Expression of IKK2ca restored total Treg and eTreg frequencies in tdLNs, but not in tumor tissue (Ext. Data Fig. 9a). It also did not restore Foxp3 expression, only partially reduced TNF and IFNγ co-expression by tumor-infiltrating CARMA1-deficient Treg, and did not

prevent their anti-tumor activity (Ext. Data Fig. 9b–d), emphasizing the importance of CBM complex effector functions other than NF-kB activation[16] in stabilizing tumor-reactive Treg.

To examine if CARMA1-deletion acutely destabilizes intratumoral Treg, we generated Foxp3$^{GFP\text{-}CreERT2}$ x CARMA1$^{f/f}$ ('F^{CreERT2} x C1$^{f/f}$') mice and treated these with tamoxifen to trigger Cre-mediated CARMA1-deletion when tumors were already established (Fig. 3a and Ext. Data Fig. 9e). To prevent subsequent recruitment of additional Treg from tdLNs we concurrently blocked lymphocyte tissue egress using the functional S1P-receptor antagonist FTY720, as described.[4] Within 2 days of treatment, tumor growth decelerated (Fig. 3b). A similarly rapid, albeit slightly less pronounced growth effect as well as increased Treg effector cytokine secretion resulted from deletion of CARMA1 in only half instead of all Treg (Ext. Data Fig. 9f–g). Intratumoral Treg destabilization was accompanied by pronounced induction of macrophage cell surface MHC class II-expression, both upon constitutive or acute deletion of either one or both alleles of *Carma1* in Treg (Fig. 3c and Ext. Data Fig. 9h). Furthermore, MHC class I-expression on tumor cells increased, predictably sensitizing them to CTL-mediated lysis (Fig. 3d). While Treg-derived IFNγ thus caused widespread tumor inflammation it also triggered tumor cell-expression of PD-L1, a ligand for the T cell inhibitory receptor PD-1, suggesting that concurrent induction of adaptive immune resistance[3] limited improved tumor control resulting from enhanced anti-tumor immune effector functions (Fig. 3d).

Considering induction of PD-L1 on tumor cells, we hypothesized that antibody-mediated blockade of PD-1 may synergize with the anti-tumor effects of IFNγ-secreting Treg. Indeed, αPD-1 therapy initiated simultaneously with CARMA1-deletion in Treg enabled much more rapid and consistent control of D4M.3A melanoma than either treatment alone (Fig. 4a). Targeting the CBM-complex in Treg may thus be highly effective at enhancing the potency of immune checkpoint therapy (ICT) in cancer patients.

While pharmacological inhibitors of the scaffold protein CARMA1 are currently not available, inhibitors of MALT1 paracaspase are predicted to attenuate the majority of CBM complex-dependent effector pathways (Fig. 4b). Indeed, similar to CARMA1-deficient mice, Treg are virtually absent in mice expressing mutant MALT1 proteins that lack paracaspase activity (replicating continual and complete pharmacological inhibition).[21–23] We therefore tested the allosteric MALT1 inhibitor mepazine[24,25] and the catalytic site binder MI-2[26] for activity against solid tumors. Both produced similar deceleration of melanoma growth as CARMA1-deletion in Treg (Fig. 4c), even when CD8$^+$ T cells were depleted (Ext. Data Fig. 9i). Systemic MALT1 inhibition will also target cells other than Treg, including melanoma cells.[27] However, no effect on tumor growth occurred in Rag1-deficient mice that lack lymphocytes (Fig. 4d). MALT1 inhibition also did not synergize with CARMA1-deletion in Treg, suggesting that its anti-tumor activity does not result from effects other than attenuated CBM complex function in Treg (Ext. Data Fig. 9j). Since MALT1 inhibition is predicted to attenuate, but not enhance lymphocyte effector functions,[28] we conclude that its impact on tumor growth is most likely mediated through destabilization of Treg. Indeed, similar to Treg-specific CARMA1-deletion, mepazine treatment caused rapid, albeit less pronounced induction of TNF- and IFNγ-expression by tumor-infiltrating Treg (Fig. 4e). Short-term in vitro treatment of Treg triggered only a minor reduction of Foxp3, GITR, and CTLA-4

expression (Ext. Data Fig. 10a) and did not induce IFN-γ-secretion (**data not shown**), indicating that the latter occurs only under the conditions of the tumor microenvironment. Accordingly, mepazine caused up-regulation of MHC I and PD-L1-expression on tumor cells in vivo (Fig. 4f) and induction of *Ifng* and a wide range of IFN-γ-regulated genes indicative of both T_H1-inflammation and adaptive immune resistance in tumor tissue (Ext. Data Fig. 10b). In contrast to constitutive CARMA1-deletion, short-term MALT1-inhibition did not reduce Treg frequency, and the expression of Treg-associated genes in tumor tissue was not reduced (Fig. 4e and Ext. Data Fig. 10c). Nevertheless, in addition to overall enhanced immune cell infiltration, mepazine treatment specifically increased the frequencies of CTL and NK cells in tumor tissue (Ext. Data Fig. 10d–h).

High tumor mutational load favors response to ICT in cancer patients,[29,30] and low mutational burden remain a major challenge that limits the success of this form of immunotherapy to some cancer types and to the minority of patients. Accordingly, D4M.3A melanoma, which carries a negligible mutational load relative to the C57BL/6J reference exome (David E. Fisher, personal communication), is completely resistant to αPD-1 monotherapy in male hosts (Fig. 4g), in contrast to female hosts where Y-antigen-expressing male D4M.3A tumors showed a partial response (Fig. 4a). Concurrent MALT1 inhibition, however, synergized with αPD-1 treatment, and arrested tumor growth even in male hosts (Fig. 4g). αPD-1 treatment did not further increase Treg-expression of IFNγ, indicating that PD-1 did not restrict the proinflammatory function of destabilized Treg (Ext. Data Fig. 10i). Furthermore, when we raised the immunogenicity of D4M.3A tumors by expressing the chicken ovalbumin-derived SIINFEKL-epitope as a surrogate mutational neoantigen, we observed an initial response to αPD-1 monotherapy, but 40% of tumors relapsed. Combination of αPD-1 antibodies with mepazine, however, produced accelerated rejection and prevented relapse (Fig. 4h). Finally, to explore effects of MALT1 inhibition on other cancer types, we treated animals implanted with MC38 colon carcinoma. While αPD-1 monotherapy had only a moderate impact on late-stage tumors, combination with mepazine enabled profound tumor control and relapse-free rejection in the majority of animals (Ext. Data Fig. 10j). Hence, systemic MALT1 inhibition inflames the tumor environment and renders poorly immunogenic tumors responsive to αPD-1 therapy while enhancing responses of immunogenic tumors and minimizing the frequency of relapse, a common problem in clinical ICT.[31]

We propose that inhibition of MALT1 protease or of other CBM complex functions could be a useful therapeutic strategy to elicit an intratumoral T_H1 autoimmune-reaction mediated by locally destabilized, preferentially self-reactive Treg. Pro-inflammatory effects of destabilized Treg appear to outweigh any potential attenuation of immune effector cell activities through MALT1 inhibition. Due to its selectivity for intratumoral Treg, this treatment may increase the fraction of cancer patients that respond to PD-1/PD-L1-targeted ICT or other forms of immunotherapy without inducing systemic autoimmune toxicity.

Methods

Mice

Foxp3$^{YFP-Cre}$ (Ref.[32]), Foxp3$^{GFP-Cre-ERT2}$ (Ref.[33]), Rosa26$^{STOP\ f/f-YFP}$ (Ref.[34]), Rosa26$^{STOP\ f/f-IKK2ca}$ (Ref.[35]), Ifng KO,[36] B6-*scurfy* (Ref.[37]) and C57BL/6/J mice were purchased from Jackson laboratories. Ramnik J. Xavier and James J. Moon (MGH) provided CARMA1$^{f/f}$ (Ref.[38]) and Rag1 KO mice, respectively. Animals were housed in specific pathogen-free facilities at the Massachusetts General Hospital (MGH) and all experimental studies were approved and performed in accordance with guidelines and regulations implemented by the MGH Institutional Animal Care and Use Committee (IACUC). For survival studies the age of mice at euthanasia mandated by a moribund state of health was recorded in Kaplan Meyer plots.

Tumor cell lines

The BRAF^{V600E} x PTEN^{null} melanoma cell line D4M.3A (Ref.[18]) was provided by David. E. Fisher. For some experiments D4M.3A were lentivirally transduced to express a blue fluorescent histone H2B-Cerulean fusion protein (D4M.3A-H2B-Cerulean), as described[39] in order to facilitate detection by flow cytometry. To generate D4M.3A-SIINFEKL tumors expressing the chicken ovalbumin-derived H-2K^{b}-restricted SIINFEKL peptide, we transduced D4M.3A cells with a VSV-G pseudotyped pHAGE-EF1α lentiviral vector engineered to express a fusion of histone H2B and Cerulean separated by two copies of the SIINFEKL minigene and its native flanking sequences in the ovalbumin protein to facilitate processing for antigen presentation. The colon adenocarcinoma cell line MC38[40] was obtained from Andrew D. Luster. All tumor lines were grown in DMEM with 10% FCS and used for experiments when in exponential growth phase.

Tumor growth studies and treatments

10^6 D4M.3A, D4M.3A-H2B-Cerulean, D4M.3A-SIINFEKL or MC38 tumor cells were s.c. injected in 100 μl HBSS w/o Ca^{2+} into the flanks of mice. Wherever possible, animals were randomized into treatment groups. Tumor volumes were measured every second to third day after start of treatments and calculated as V = (length x width^2)/2.

1 mg/mouse of tamoxifen in 100 μl of a 9:1 mixture of olive oil and ethanol was i.p. injected daily as indicated. 1 mg/kg bodyweight of FTY720 in 150 μl H_2O was i.p. injected every other day until the end of the experiment. 500 μg/mouse of αIFNγ antibody (clone XMG1.2) per mouse was i.p. injected on day 14 after birth or on the day of tumor implantation and then every other day thereafter until the end of the experiment. 200 μg of αPD1 (clone 29F.1A12) or of rat IgG2a isotype control (clone 2A3) were i.p. injected three times in 100 μl PBS every other day at the indicated time-points. 150 μg of αCD8α (clone YTS169.4) were i.p. injected in 100 μl PBS every other day from the indicated time-point until the end of the experiment. 16 mg/kg bodyweight of Mepazine in 5% DMSO or 20 mg/kg of MI-2 in 5% DMSO in purfied H_2O were i.p injected daily starting at the indicated time-points until the end of the experiment, unless indicated otherwise. For adoptive Treg cell transfer studies, CD4$^+$ YFP$^+$ Treg were purified to >95% purity through magnetic-activated cell sorting (Miltenyi) from LNs and spleen of Foxp3$^{YFP-Cre}$ x CARMA1$^{f/+}$ of

CARMA1$^{+/+}$ mice and 10^6 cells/mouse i.v. injected into the tail vein the day before tumor implantation.

Preparation of single cell suspensions, antibody staining and flow cytometry

Heparinized peripheral blood collected through sub-mandibular vein puncture was treated with ACK red blood cell lysis buffer. LNs and spleens were passed through 40 μm cell strainers, followed by red blood cell lysis (spleens only). Tumors and lung tissue were minced into small fragments and treated with 1.5 mg/ml collagenase IV and 50 U/ml DNAse I for 30 min. at 37°C under agitation. Skin tissue was digested in medium containing 2% FCS, 10mM Hepes, 0.5 mg/ml hyaluronidase, 1.5 mg/ml collagenase IV, and 50 U/ml DNAse I for 45 min. at 37°C under agitation. Residual tissue fragments were mechanically dissociated.

Cell surface proteins were stained for 20 minutes at 4°C with the following antibodies: αCD11b (M1/70), CD120b/TNFR2 (polyclonal Armenian hamster IgG), CD274/PD-L1 (10F.9G2), CD357/GITR (DTA-1), CD4 (GK1.5), CD45 (30-F11), CD62L (MEL-14), CD73 (TY/11.8), CD8α (53–6.7), CD90.2 (30-H12), F4/80 (BM8), H-2K^b (AF6–88.5), -I-A/I-E (M5/114.15.2), Ly-6C (HK1.4), Ly-6G (1A8), CD45R/B220 (RA3–6B2), CD64 (FcγRI) (X54–5/7.1), CD11c (N418), CD103 (2E7), NK-1.1 (PK136), CD335 (NKp46) (29A1.4), CD3 (17A2), CD19 (1D3/CD19), CD45RB (16A), and CD44 (IM7) (BioLegend), CD11c (HL3) and CD25 (PC61.5) (eBIoscience).

Intracellular and nuclear proteins were stained for 60 minutes at room temperature after permeabilization and fixation (Mouse regulatory T cell staining Kit; eBioscience) using antibodies against: CD152/CTLA-4-(UC10–4B9), TNF (MP6-XT22), IL-4 (11B11), IL-17A (TC11–18H10.1), IFNγ (XMG1.2), Tbet (4B10), and Ki67 (16A8) (BioLegend), BIM (C34C5), CARD11/CARMA1 (1D12) (Cell Signaling), Foxp3 (FJK-16s, eBioscience), GATA3 (L50–823) and Ki67 (B56) (BD Biosciences), RORγt (AFKJS-9) and GFP (rabbit polyclonal) (Invitrogen). Polyclonal goat α-rabbit Ig (H+L) secondary antibody (Life Technologies) was used to reveal primary αCARMA1 staining.

Preceding antibody staining, dead cells where stained using the fixable viability violet dye Zombie Red (Biolegend) for 15 minutes at room temperature, followed by blocking of Fc receptors with TruStain FcX (Biolegend) for 20 minutes at 4°C. Cells were analyzed on LSR II, LSRFortessa or LSRFortessa X-20 flow cytometers (BD Biosciences), and data were analyzed with FlowJo software version 9.9.5.

Phospho-protein analysis

LN single cell suspensions were stained using the fixable viability dye ZombieRed (Biolegend) for 15 min. at room temperature, and added for 30 minutes at 37°C to tissue culture plates pre-coated overnight with αCD3ε (clone 145–2C11) and αCD28 (clone 37.51) antibodies (at 10 μg/ml of each antibody), or to uncoated control plates. Samples were then fixed in 4% paraformaldehyde (PFA) for 10 minutes at room temperature, and permeabilized for 20 minutes through dropwise addition of 1 ml ice-cold methanol. Cells were then stained for CD90.2 (30-H12), CD4 (GK1.5), CD8α (53–6.7), CD44 (IM7)

(BioLegend), Foxp3 (FJK-16s, eBioscience), pFoxo1 (Thr24)/Foxo3a (Thr32), p-c-Jun (Ser73) (D47G9) (Cell Signaling) and GFP (rabbit polyclonal Ab) (Invitrogen).

Analysis of in situ and ex vivo stimulated cytokine secretion

To detect in situ cytokine secretion, mice were slowly i.v injected with 500 μg of Brefeldin A in 250 μl PBS 6 h before sacrifice and intracellular cytokine staining.

To detect cytokine secretion in T cells upon ex vivo re-stimulation, single cell suspensions from tumors and LNs were resuspended in RPMI 1640 with 10% FCS and added to αCD3 (clone 145–2C11)/αCD28 (clone 37.51) antibody-coated (overnight at 10 μg/ml antibody) tissue culture plates for 8 hours at 37°C in the presence of 1 μg/mL Golgiplug and Monensin (both from Biolegend) and cells processed for intracellular cytokine staining.

Analysis of exTreg

$CD4^+$ YFP^{bright} cells were first purified by FACS from LNs and spleens of $Foxp3^{YFP\text{-}Cre/+}$ x $CARMA1^{f/f\ (or\ f/+\ or\ +/+)}$ x $Rosa26^{YFP}$ mice and stained for Foxp3 expression for flow cytometry analysis, as described above.

In vivo and in vitro suppression

For in vivo suppression studies, 3×10^5 Miltenyi (negative selection) enriched $CD4^+$ and FACS sorted (>98% purity) $CD45RB^{high}$ YFP^- cells from LNs and spleens of $Foxp3^{YFP\text{-}Cre/Cre}$ mice were i.v. injected into the tail vein of Rag1 KO mice with or without 1×10^5 Miltenyi (negative selection) enriched $CD4^+$ and FCAS sorted (>98% purity) YFP^{bright} Treg cells from LNs and spleens of $Foxp3^{YFP\text{-}Cre/+}$ x $CARMA1^{f/f\ (or\ f/+\ or\ +/+)}$ x $Rosa26^{YFP}$ mice.

For in vitro suppression studies, 1×10^4 FACS sorted (>98% purity) $CD4^+$ YFP^- conventional T cells from LNs and spleens of $Foxp3^{YFP\text{-}Cre/Cre}$ mice were labeled with 5 μM CellTrace Violet and stimulated with 250 ng/ml of αCD3 mAb (145–2c11, Biolegend) in presence of 2.5×10^4 T-cell depleted splenocytes and different concentrations (from 1:1 to 1:16) of Miltenyi (negative selection) enriched $CD4^+$ and FACS sorted (>98% purity) YFP^{bright} Treg cells from LNs and spleens of $Foxp3^{YFP\text{-}Cre/+}$ x $CARMA1^{f/f\ (or\ f/+\ or\ +/+)}$ x $Rosa26^{STOP\ f/f\text{-}YFP}$ mice. $CD4^+$ YFP^- conventional T cell proliferation was read out after 72h, as previously described.[41] Briefly, percentage of suppression was scaled from 0 (proliferation of conventional T cell in absence of Treg) to 100 (complete absence of proliferation).

In vitro apoptosis

Enriched $CD4^+$ and FACS-purified (>99% purity) YFP^{bright} Treg cells from LNs of $Foxp3^{YFP\text{-}Cre/+}$ x $CARMA1^{f/f\ or\ +/+}$ x $Rosa26^{STOP\ f/f\text{-}YFP}$ mice were added for 6 and 18 hrs at 37°C to tissue culture plates pre-coated overnight with αCD3ε (clone 145–2C11) and αCD28 (clone 37.51) antibodies (at 10 μg/ml of each Ab). Viability of $CD44^{lo}$ $CD62L^+$ cTreg and $CD44^{hi}$ $CD62L^{neg}$ eTreg was then read out by Annexin V and Zombie Red staining (Biolegend).

RNA-Sequencing studies

Sample collection.—$CD4^+$ T cells from LNs and spleens of $F^{Cre/+}$ x $C1^{+/+, f/+, or f/f}$ mice were pre-enriched by immunomagnetic cell sorting (Miltenyi negative selection) and then 5 × 10^3 YFP^+ $CD4^+$ $CD44^{lo}$ $CD62L^+$ cTreg/animal and the same number of YFP^+ $CD4^+$ $CD44^{hi}$ $CD62L^{neg}$ eTreg sorted to >99% purity directly into 10 μL lysis buffer consisting of TCL buffer (Qiagen) and 1% of beta-mercaptoethanol. Samples were the flash frozen and kept at −80°C prior to further processing following a modified version of the Smart-Seq2 protocol, [11–13] as described below. A total of 18 samples were collected, but 2 samples were discarded for technical reasons.

Reverse transcription.—Samples were thawed on ice for 2 minutes, then centrifuged at 2,500 rpm at 4°C for 1 minute and the RNA concentration normalized. 1.9 μL of RNA per sample were moved to a full-skirt 96-well plate (Eppendorf). Each sample was then mixed with 1μL 10μM RT primer 5'AAGCAGTGGTATCAACGCAGAGTACTTTTTTTTTTTTTTTTTTTTTTTTTTTTV N-3' (IDT), 1μL 10 mM dNTP (Life Technologies/Thermo Fisher Scientific), and 0.1μL SUPERase•In RNase-Inhibitor (20 U/μL, Life Technologies/Thermo Fisher Scientific). Samples were denatured at 72° C for 3 minutes using an Eppendorf Mastercycler and placed immediately on ice afterwards. 7 μL of the Reverse Transcription Mix was subsequently added to every well, consisting of: 2 μL 5x RT buffer (Thermo Fisher Scientific), 2 μL 5 M Betaine (Sigma-Aldrich), 0.9 μL 100 mM MgCl2 (Sigma-Aldrich), 1 μL 10 μM TSO (5'-AAGCAGTGGTATCAACGCAGAGTACATrGrG+G-3', Exiqon), 0.25 μL SUPERase•In RNase-Inhibitor (20U/μL, Life Technologies/Thermo Fisher Scientific), 0.1 μL Maxima H Minus Reverse Transcriptase (200U/μL, Thermo Fisher Scientific), and 0.75 μL nuclease-free water. Reverse transcription was carried out by incubating the plate at 50°C for 90 minutes, followed by heat inactivation at 85°C for 5 minutes.

PCR pre-amplification and cDNA purification.—14 μL of PCR Mix, consisting of 0.5 μL 10 μM PCR primer 5'-AAGCAGTGGTATCAACGCAGAGT-3' (IDT), 12.5 μL 2x KAPA HiFi HotStart ReadyMix (KAPA Biosystems), and 1μL nuclease-free water, was added to each well for a final PCR reaction volume of 25 μL. The reaction was carried out with an initial incubation at 98°C for 3 minutes, followed by 16 cycles at (98°C for 15 seconds, 67°C for 20 seconds, and 72°C for 6 minutes) and a final extension at 72°C for 5 minutes. PCR products were purified by mixing them with 20 μL (0.8X) of Agencourt AMPureXP SPRI beads (Beckman-Coulter), followed by a 6 minutes incubation period at room temperature. The plate was then placed onto a magnet for 6 minutes prior to removing the supernatant. SPRI beads were washed twice with 100 μL of freshly prepared 70% ethanol, with care being taken to avoid loss of beads during the washes. Upon removing all residual ethanol traces, SPRI beads were left to dry at room temperature for 10 minutes. The beads were then resuspended in 20 μL of TE buffer (Teknova) and incubated at room temperature for 5 minutes. The plate was placed on the magnet for 5 minutes prior to transferring the supernatant containing the amplified cDNA to a new 96-well plate. This cDNA SPRI clean-up procedure was repeated a second time to remove all residual primer dimers. The concentration of amplified cDNA was measured on the Synergy H1 Hybrid Microplate Reader (BioTek) using the Qubit dsDNA High Sensitivity Assay Kit (Life

Technologies/Thermo Fisher Scientific). The cDNA size distribution of few selected wells was assessed on a High-Sensitivity Bioanalyzer Chip (Agilent), and the expected size distribution sharply peaked around 2 kb.

Sequencing library preparation.—Library preparation was carried out using the Nextera XT DNA Sample Kit (Illumina) with custom indexing adapters, allowing the 18 libraries to be simultaneously generated in a 384-well PCR plate (Eppendorf). For each library, the amplified cDNA was normalized to a 0.15 – 0.20 ng/μL concentration range. The tagmentation reaction consisted of mixing 0.625 μL of normalized cDNA with 1.25 μL of Tagmentation DNA (TD) Buffer and 0.625 μL of Amplicon Tagment enzyme Mix (ATM). The 2.5 μL reaction was incubated at 55°C for 10 minutes and then immediately placed on ice upon completing this incubation step. The reaction was quenched with 0.625 μL of Neutralize Tagment (NT) Buffer and incubated at room temperature for 10 minutes. The libraries were amplified by adding 1.875 μL of Nexstera PCR Master (NPM) Mix, 0.625 μL of 10 μM i5 adapter 5'-AATGATACGGCGACCACCGAGATCTACAC**[i5]**TCGTCGGCAGCGTC-3' (IDT), where **[i5]** signifies the 8 bp i5 barcode sequence (see below for sequences), and 0.625 μL of 10μM i7 adapter 5'CAAGCAGAAGACGGCATACGAGAT**[i7]**GTGACTGGAGTTCAGACGTGTGCTCTTCCGATCTGGG-3' (IDT), where **[i7]** represents the reverse-complement of the 8 bp i7 barcode sequence (see below for sequences used). The PCR was carried out at an initial incubation at 72°C for 3 minutes, 95°C for 30 seconds, followed by 12 cycles of (95°C for 10 seconds, 55°C for 30 seconds, 72°C for 1 minute), and a final extension at 72°C for 5 minutes. Following PCR amplification, 2.5 μL of each library were pooled together in a 1.5 mL Eppendorf tube. The pool was mixed with 67.5 μL (0.9X ratio for 2.5 ul of 30 samples pooled together) of Agencourt AMPureXP SPRI beads (Beckman-Coulter) and incubated at room temperature for 5 minutes. The pool was then placed on a magnet (DynaMag-2, Life Technologies) and incubated for 5 minutes. The supernatant was removed and the SPRI beads were washed twice with 1mL of freshly prepared 70% ethanol. Upon removing all residual ethanol traces, the SPRI beads were left to dry at room temperature for 10 minutes. The beads were resuspended in 100 μL of nuclease-free water and incubated at room temperature for 5 minutes. The tube was then placed back on the magnet for 3 minutes prior to transferring the supernatant to a new 1.5 mL Eppendorf tube. This SPRI clean-up procedure of the library was repeated a second time to remove all residual primer dimers, using the same approach. The concentration of the pooled libraries was measured using the Qubit dsDNA High Sensitivity Assay Kit (Life Technologies/Thermo Fisher Scientific), and the library size distribution measured on a High-Sensitivity Bioanalyzer Chip (Agilent), showing the expected size distribution of 300–500 bp. The 18-pooled samples were sequenced as paired-end on an Illumina NextSeq 500 instrument using the NextSeq 500/550 High Output v2 kit (75 cycles).

i5 barcodes: AAGTAGAG, ACACGATC, TGTTCCGA

i7 barcodes: GAATTGCT, GTCAAGTT, ATCCGACA, CAAGGCGA, AGTGTCTT, GACCGAGA

RNA Sequencing Analysis.—Raw sequencing reads were demultiplexed and converted to FASTQ files using Illumina bcl2fastq2 Illumina software (version 2.17.1.14). FASTQ sequencing reads were then aligned to mm10 reference genome using the STAR aligner with default parameters.[42] RSEM (version 1.2.8) was used to quantify gene expression level from aligned reads and generate count expression matrices for each experimental condition.[43] We filtered out lowly expressed genes with a count per million (CPM) < 0.5 in more than 2 conditions, leaving a total of 14168 genes for further analysis. Distribution of log2 normalized CPM data was visualized to assess for coverage, and all conditions had similar distributions.

Gene Expression Analysis.—Gene expression matrices were analyzed using the limma package in R.[44] The global topology of quantile normalized data was visualized using the multidimensional scaling (plotMDS) function in limma after removing batch effects using the removebatchEffect function in limma with default parameters taking into account design and batch matrices. Differential gene expression was performed using empirical Bayesian statistics (eBayes) function in limma simultaneously correcting for batch using blocking terms for batch covariates. Differentially expressed genes with log fold change greater than 1 and a p-value below cut-off were visualized using the heatmap.2 function in gplots. All p values were corrected for multiple hypothesis testing using Benjamini-Hochberg correction. For R scripts used to perform the gene expression analyses see Supplementary Material and Methods. The same differential expression steps were used to re-analyze the gene expression data from GSE82008 in order to obtain the list of differentially expressed genes between c-Rel KO and p65 KO vs WT resting and activated Tregs. A list of 831 ‘eTreg signature’ genes from Grinberg-Bleyer et al. was obtained through direct correspondence with the authors. Overlap between differentially expressed genes, including the list of eTreg signatures from the current study and Grinberg-Bleyer et al., was visualized using the vennDiagram function in limma.

Quantitative RT-PCR

For analysis of gene expression, RNA was isolated (AllPrep, DNA/RNA Mini kit; Qiagen) from $CD4^+$ GFP^+ Treg sorted to >99% purity from tdLNs and tumors, or from homogenized tumor tissue, and reverse transcribed using iScript cDNA Synthesis Kit (Bio-RAD). Quantitative RT-PCR was performed using iQ SYBR green supermix (Bio-RAD) and primers: CARMA1-Fwd 5’-ACATGCTGAGCCGTTACATCA-3’, CARMA1-Rev 5’-CCACATAGCCCCTTTGTCCC-3’, Ifng-Fwd 5’-CGGCACAGTCATTGAAAGCCTA-3’, Ifng-Rev 5’-GTTG CTGATGGCC TGATTGTC-3’, CTLA4-Fwd 5’-GCTTCCTAGATTACCCCTTCTGC-3’, CTLA4-Rev 5’-CGGGCATGGTTCTGGATCA-3’, CD25-Fwd 5’-CCACATTCAAAGCC CTCTCCTA-3’, CD25-Rev 5’-GTTTTCCCACACTTCATCTTGC-3’, Foxp3-Fwd 5’-TTGG CCAGCGCCA TCTT-3’, Foxp3-Rev 5’-TGCCTCCTCCAGAGAGAAGTG-3’, GITR-Fwd 5’-AAGGTTCA GAACGGAAGTG-3’, GITR-Rev 5’-GGGTCTCCACAGTGGTACT-3’, CD73-Fwd 5’-CAA ATCCCACACAACCACTG-3’, CD73-Rev 5’-TGCTCACTTGGTCACA GGAC-3’, Gzmb-Fwd 5’-CATGTAGGGTCGAGAGTGGG-3’, Gzmb-Rev 5’-CCTCCTGC TACTGCTGAC CT-3’, Pdl1-Fwd 5’-TGCTGCATAATCAGCTACGG-3’, Pdl1-Rev 5’-GCTGGTCACATT GAGAAGCA-3’, Socs1-Fwd 5’-ACAAGCTGCTACAACCAGG G-3’,

Socs1-Rev 5'-ACT TCTGGCTGGAGACCTCA-3', Tap1-Fwd 5'-GTGGCCGCAGTGGGA CAAGAG-3', Tap1-Rev 5'-AGGGCACTGGTGGCATCATC-3', Stat1-Fwd 5'-TGGTGAAATTGCAAG AGCTG-3', Stat1-Rev 5'-CAGACTTCCGTTGGTGGATT-3', Irf1-Fwd 5'-CAG AGGAAAG AGAGAAAGTCC-3', Irf1-Rev 5'-CACACGGTGACAGTGCTGG, Cxcl10-Fwd 5'-CATC CTGCTGGGTCTGAGTG-3', Cxcl10-Rev 5'-ATTCTCACTGGCCCGTCATC, Nos2-Fwd 5'-CAAGAGAGTGCTGTTCCAGGT-3' and Nos2-Rev 5'-GAGCACGCTGAGTACC TCATT-3', GAPDH-Fwd 5'-TGGTGAAGGTCGGTGAAC-3' and GAPDH-Rev 5'-CC ATGTAGTTGAGGTCAATGAAGG-3'. Results were expressed as $2^{-\Delta CT}$ relative to the house keeping gene *Gapdh*.

Histology

Tissue samples obtained from all organs were fixed in 10% buffered formalin for 48 h, trimmed and placed into microcassettes, and embedded in paraffin wax. Sections of 5 μm were stained with haematoxylin and eosin according to standard procedures.

Immunofluorescence

Kidney, liver, and stomach from a RAG1 KO mouse were embedded in OCT and flash frozen in cold methylbutane equilibrated on dry ice. Sections of 10 μm were permeabilized with pre-cooled 90% methanol for 10 minutes at −20°C, blocked in TruStain FcX (93, Biolegend) with 1% goat serum and 0.25% BSA in PBS for 60 minutes, incubated with sera (1:100 dilution) from $Foxp3^{YFP\text{-}Cre/Y}$ x $CARMA1^{f/f\ (or\ f/+\ or\ +/+)}$ mice for 120 minutes and stained with anti-mouse IgG (H+L)-Alexa Fluor647 (1:500) (A-21235, Thermo Fisher) and DAPI (Sigma) for 120 minutes. Sections were mounted on coverslips in Prolong (Thermo Fisher) and imaged with LSM 780 AxioObserver confocal microscope (Carl Zeiss) using a 20x lens (Apochromat, 0.8 W).

Statistical analysis

Two-tailed student's t-test was used for comparisons between two groups while two-way ANOVA with Bonferroni post-test (multiple time-points) or one-way ANOVA with Tukey post-test (single time-points) were used for comparisons across multiple groups, unless otherwise indicated. A log-rank (Mantel–Cox) test was used to compare survival curves. All statistical tests were performed with GraphPad Prism software, and $p < 0.05$ was considered statistically significant. No statistical methods were used to predetermine sample size. Investigators were not blinded to allocation during experiments and outcome assessment.

Extended Data

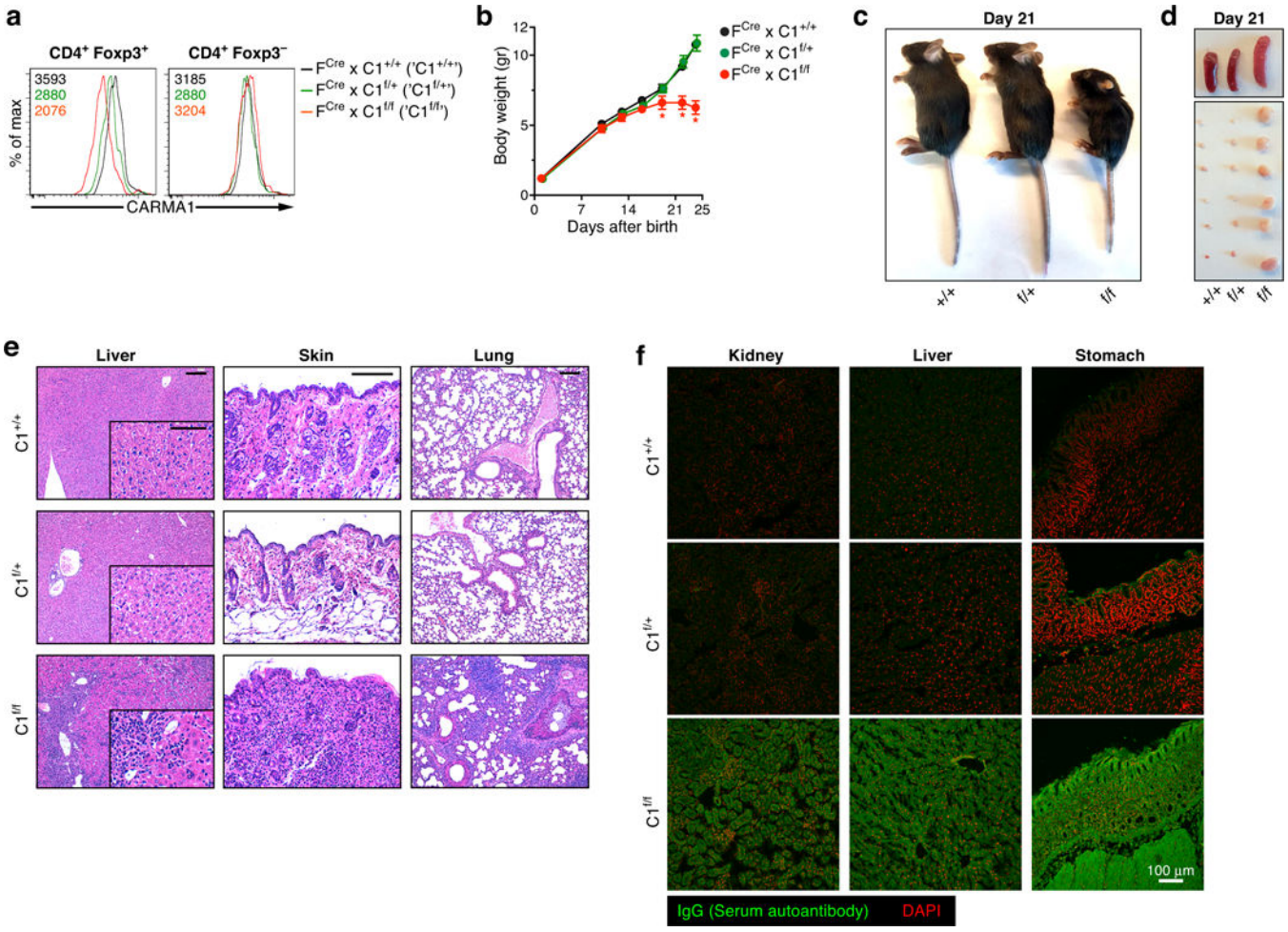

Extended data Figure 1. Lymphoproliferative disease upon Treg-specific deletion of CARMA1.

a, CARMA1-protein in Treg and CD4^{+} Tconv from LNs of Foxp3$^{YFP\text{-}Cre}$ x CARMA1$^{+/+}$, CARMA1$^{f/+}$, and CARMA1$^{f/f}$ mice ('F^{Cre} x C1$^{+/+,\ f/+,\ f/f}$'). **b**, Weight curves (n=5/group) **c-d,** Appearance of 21 day-old animals (c), their spleens and LNs (d). **e,** Histological appearance of liver, skin, and lung at 21 days of age of indicated mice. Scale bars indicate 150 µm and 50 µm (insets), respectively. **f**, Kidney, liver, and stomach tissue sections of healthy C57BL/6 Rag KO mice were reacted with serum from 21 days old mice of the indicated genotypes, and self tissue-reactive IgG revealed by α-mouse IgG staining (green). Nuclei were stained with DAPI (red).

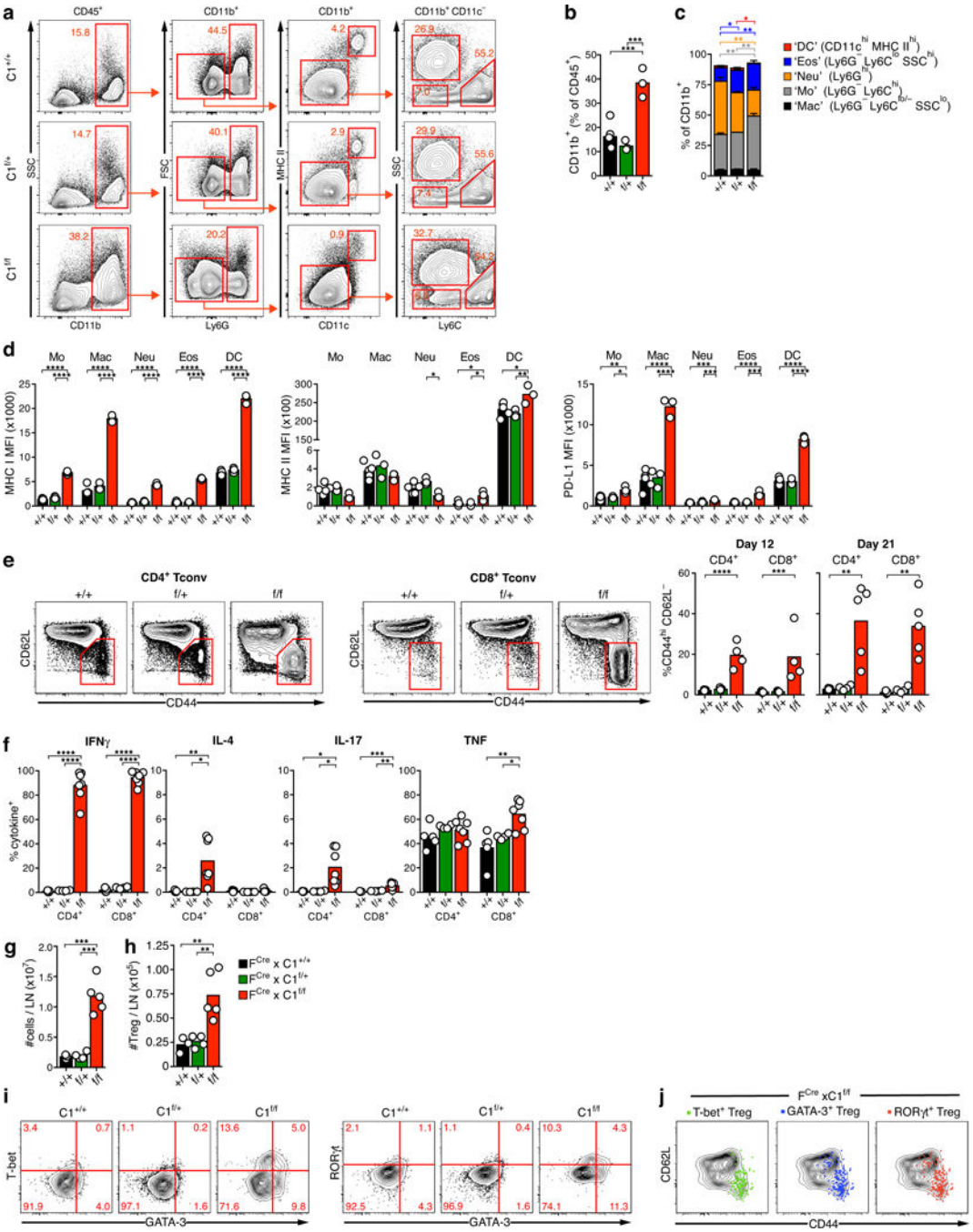

Extended data Figure 2. Lymphoproliferative disease upon Treg-specific deletion of CARMA1 (cont'd).

a-c, Size of the CD11b^{+} splenic myeloid compartment and proportions of Ly6G^{+} neutrophils, CD11c^{+} MHC II^{hi} DCs, Ly6C^{hi} monocytes, Lyc6G^{lo} SSC^{hi} eosinophils, and Ly6C^{lo} SSC^{lo} macrophages in F^{Cre} x C1$^{+/+,\ f/+,\ f/f}$ mice. **d**, Expression of MHC I, MHC II, and PD-L1 on splenic myeloid subsets. **e,** Frequency of CD4^{+} and CD8^{+} Tconv with a CD44^{hi} CD62L^{-} effector memory phenotype in LNs of indicated mice at age 12 and 21 days. **f**, Effector cytokine expression of Tconv from 21-day old mice upon 8-hour ex vivo

stimulation on αCD3/CD28-coated plates. **g**, LN cellularity. **h**, Absolute numbers of Treg in LNs. **i,** Co-expression of indicated transcription factors by Treg from LNs of indicated mice. **j**, Expression of CD44 and CD62L by F^{Cre} x $C1^{f/f}$ Treg expressing T-bet (green dots), GATA-3 (blue dots), or RORγt (red dots), compared to total $C1^{f/f}$ Treg (contour plots). */**/***/**** = $p<0.05/0.01/0.001/0.0001$.

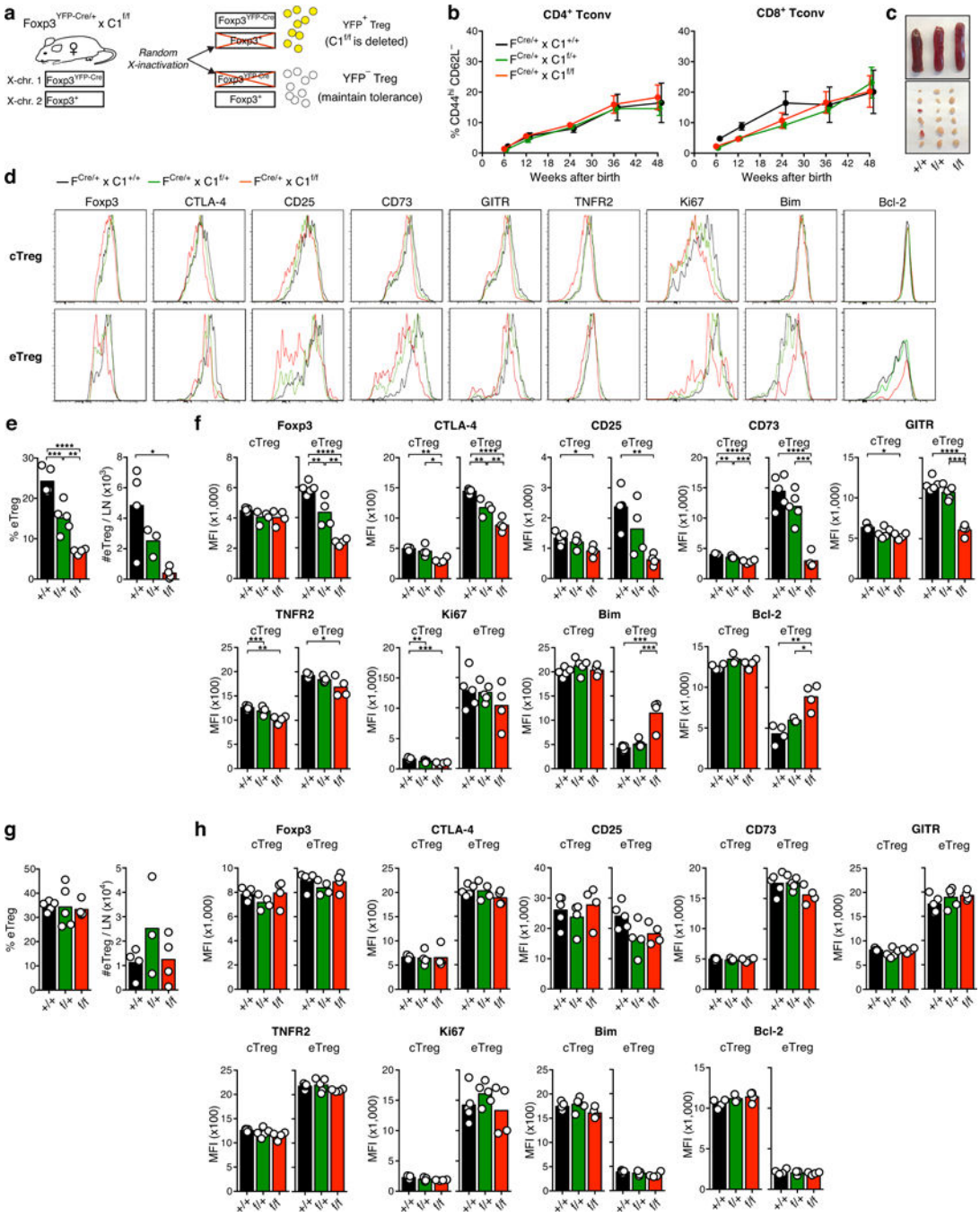

Extended data Figure 3. Role of CARMA1 in eTreg differentiation.

a, Female heterozygous Foxp$^{YFP\text{-}Cre/+}$ ('F$^{Cre/+}$') x CARMA1$^{f/f}$ mice express YFP-Cre and delete CARMA1$^{f/f}$ in half of Treg due X-chomosomal location of the Foxp3$^{YFP\text{-}Cre}$ allele and random X chromosome inactivation, while the other half of Treg remains functional. **b**, Frequency of CD4^{+} and CD8^{+} Tconv with a CD44^{hi} CD62L^{-} effector memory phenotype in peripheral blood of aging F$^{Cre/+}$ x C1$^{+/+,\ f/+,\ or\ f/f}$ mice (n=4/group). **c,** Appearance of spleens and LNs of indicated mice at 1 year of age. **d-f**, Frequency and absolute numbers (e) of eTreg and expression of Foxp3, indicated markers of eTreg differentiation, as well as

proliferation marker Ki67, pro-apoptotic protein Bim and anti-apoptotic protein Bcl-2 by YFP^+ cTreg and eTreg (d, f) from 9-week old $F^{Cre/+}$ x $C1^{+/+,\ f/+,\ or\ f/f}$ mice. *Note*: Some data on eTreg in e-f are the same as shown in Fig. 1g–h and shown to facilitate comparison to cTreg and YFP^- Treg in g-h. **g-h**, Frequency and absolute numbers of eTreg (g) and eTreg markers on YFP^- cTreg and eTreg (h) from the same animals as shown in d and f. */**/***/**** = $p<0.05/0.01/0.001/0.0001$.

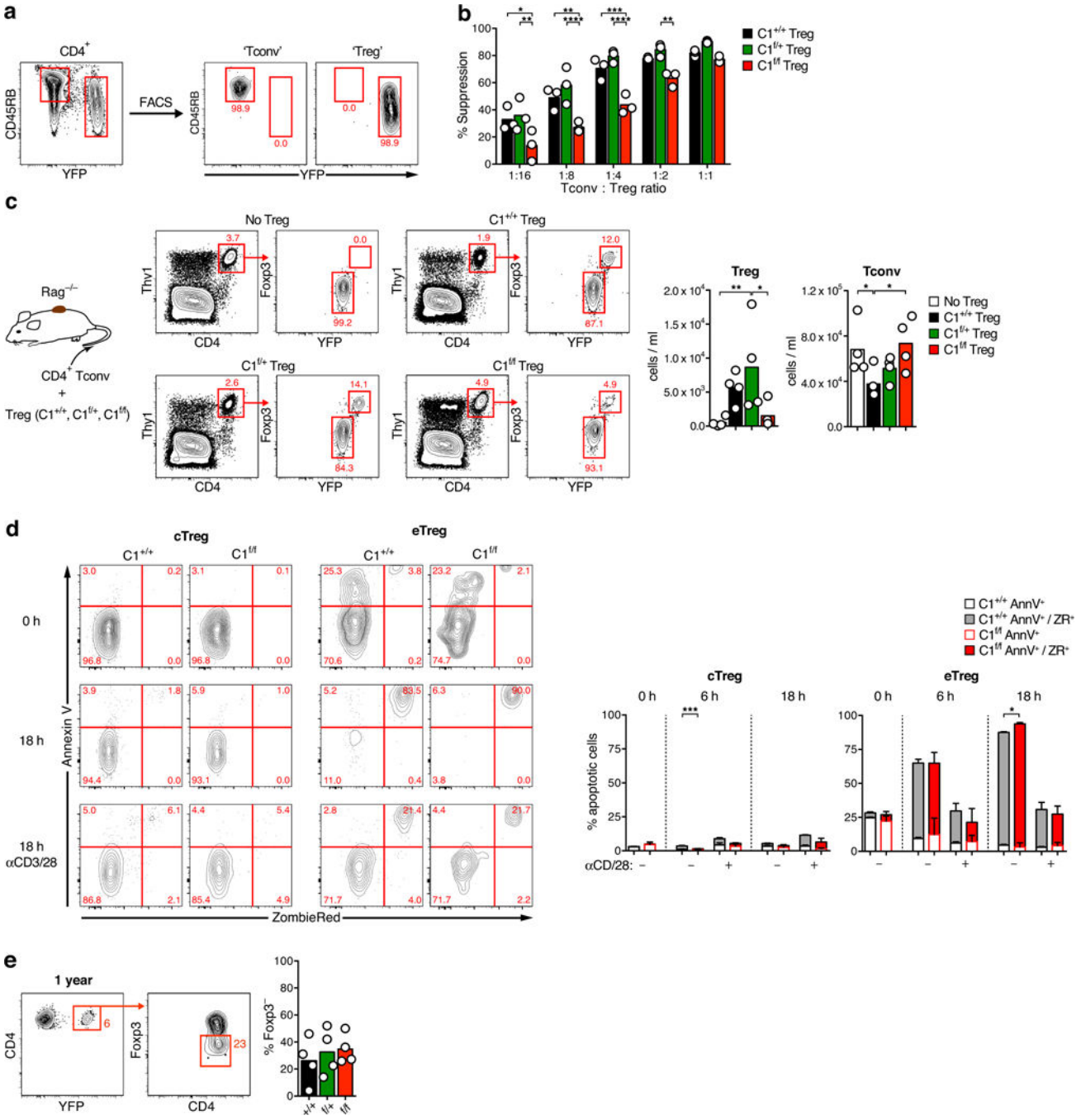

Extended data Figure 4. In vitro and in vivo suppression, apoptotic rate, and exTreg formation of CARMA1-deficient Treg.

a, $CD4^+$ $CD45RB^{hi}$ YFP^- Tconv and $CD4^+$ $CD45RB^{lo}$ YFP^{bright} Treg were double-sorted to >98% purity from LNs and spleens of F^{Cre} x $C1^{+/+}$ x $Rosa26^{STOP\ f/f\text{-}YFP}$ mice, which allow for clear differentiation of Cre-expressing Treg based on high expression of soluble EYFP in addition to the YFP-Cre fusion protein. **b**, YFP^{bright} Treg from F^{Cre} x $C1^{+/+}$ or $F^{Cre/+}$ x $C1^{f/+\ or\ f/f}$ mice and CellTrace Violet-labeled Tconv from F^{Cre} x $C1^{+/+}$ mice were co-cultured at indicated ratios for 3 days in the presence of αCD3 Abs and T-depleted

splenocytes and suppression measured as reduction of Tconv proliferation. **c**, Treg of various genotypes and Tconv were co-adoptively transferred into Rag-deficient hosts and their respective frequency in peripheral blood determined 8 weeks later. **d**, $CD4^+$ YFP^+ Treg of indicated genotypes were cultured without exogenous IL-2 on αCD3/CD28-coated or uncoated plates for 6 or 18 hours and examined for reactivity with AnnexinV and the viability dye ZombieRed. **e**, $CD4^+$ YFP^{bright} cells were sorted from LNs of 1-year old and $F^{Cre/+}$ x $C1^{+/+,\ f/+,\ or\ f/f}$ x $Rosa26^{STOP\ f/f\text{-}YFP}$ mice and subsequently stained for expression of Foxp3 protein to determine the frequency of $Foxp3^-$ 'exTreg'. * = $p<0.05$, ** = $p<0.01$, *** = $p<0.001$, and **** = $p<0.0001$. 2-way ANOVA with Sidak post-test was used in a.

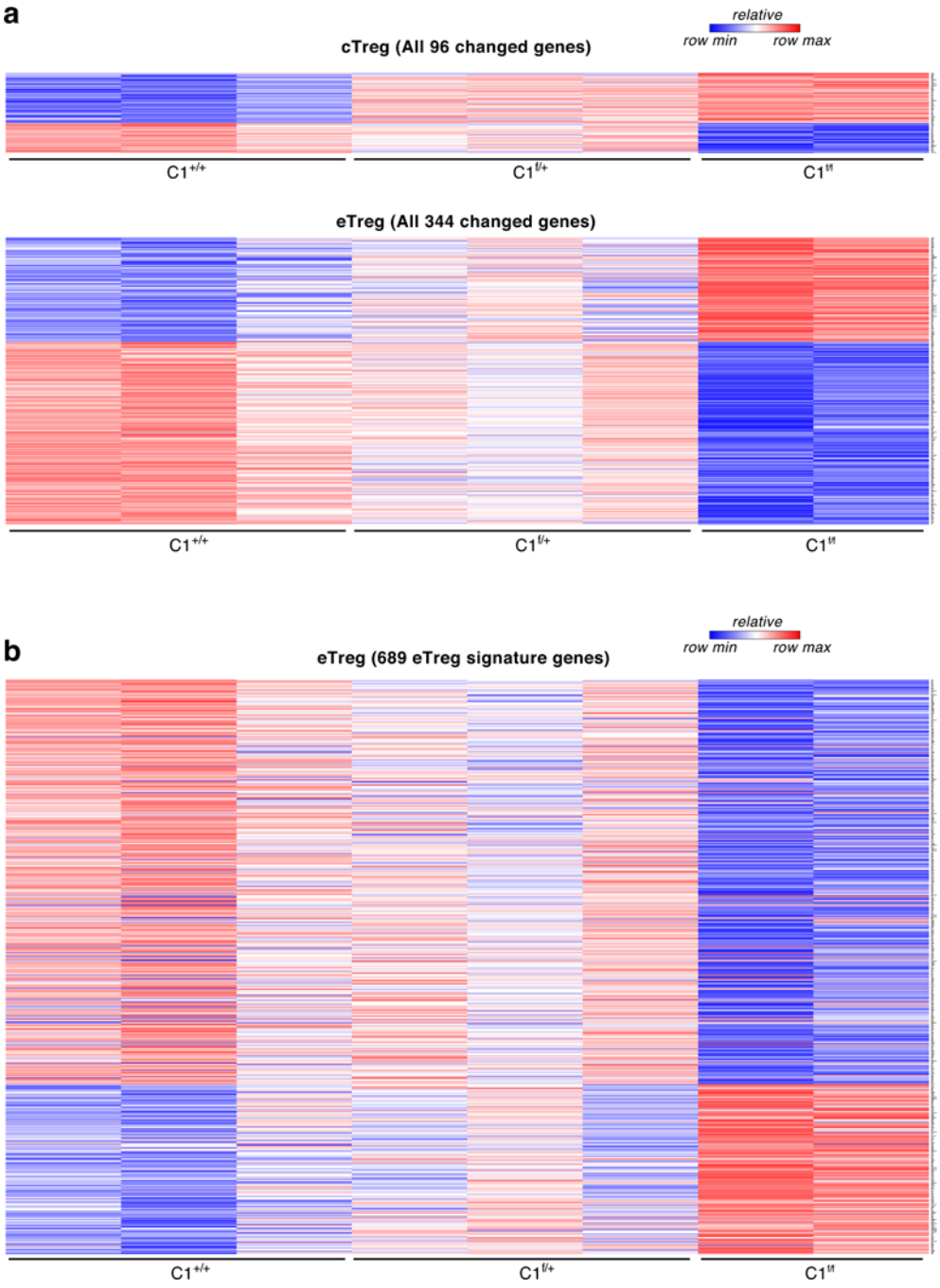

Extended data Figure 5. Bulk RNA-seq analysis of YFP^{+} cTreg and eTreg from LNs of F$^{Cre/+}$ x C1$^{+/+}$, C1$^{f/+}$, and C1$^{f/f}$ mice.

a, Scaled expression in cTreg (top) and eTreg (bottom) of genes differentially expressed (fold change > 2 and $p_{adj} < 0.05$) between C1$^{+/+}$ and C1$^{f/f}$ mice. **b**, High-resolution, fully annotated heatmap of eTreg signature genes as shown in Fig. 1j.

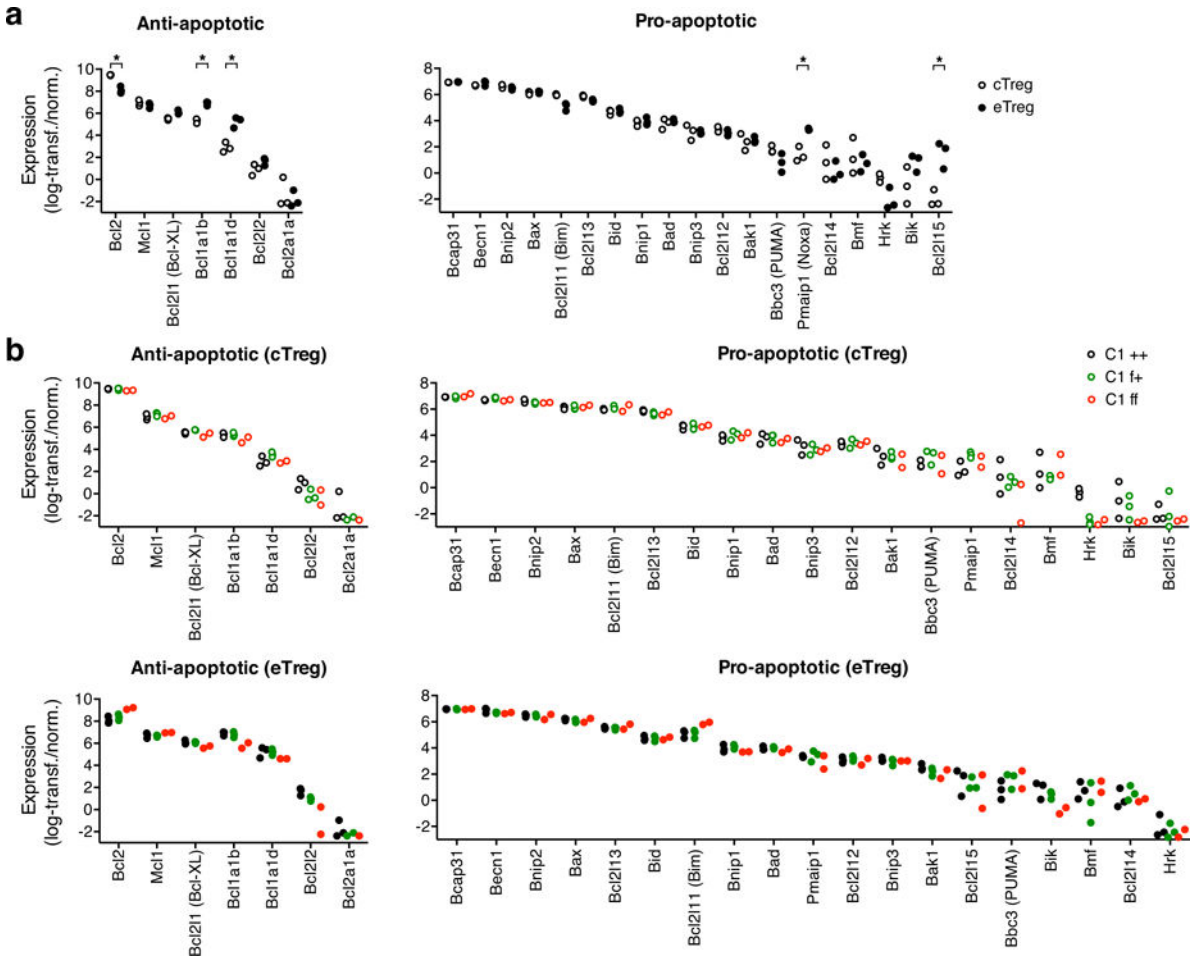

Extended data Figure 6. Expression of apoptotic regulator genes.

a, Comparison of normalized, log-transformed mRNA expression levels of anti- and pro-apoptotic Bcl2 family genes in YFP^+ cTreg and eTreg from $F^{Cre/+}$ x $C1^{+/+}$ mice, based on RNA-Seq analyses. **b**, Comparison of expression of the same genes in cTreg (top) and eTreg (bottom) of the indicated genotypes. *: $p_{adj} < 0.05$

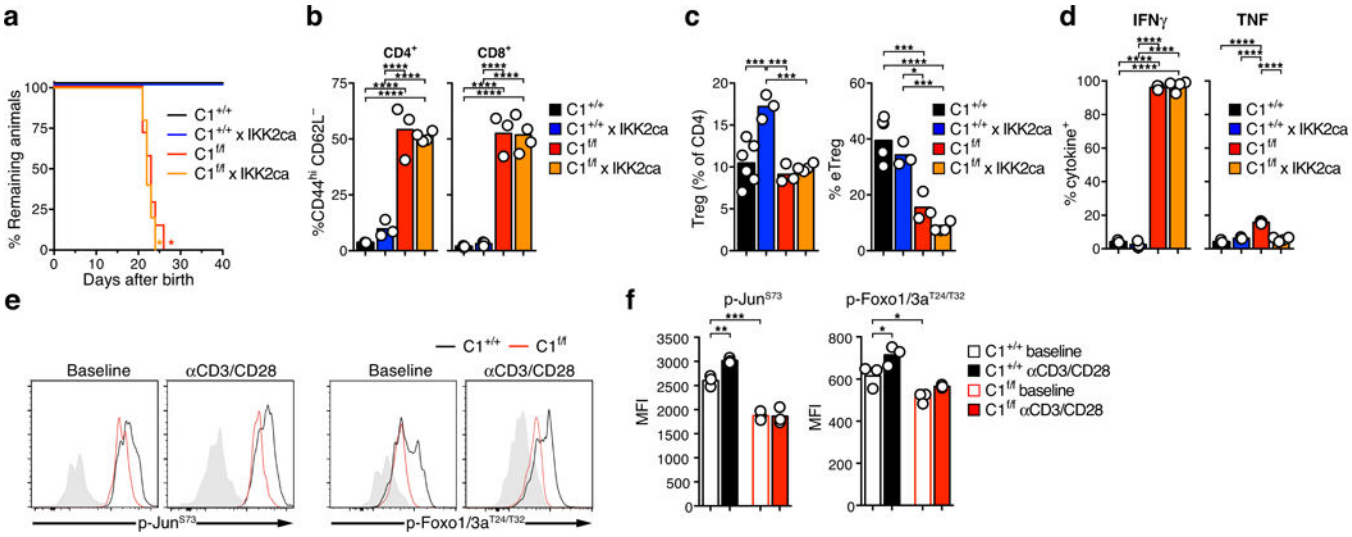

Extended data Figure 7. Restoring NF-κB activation in CARMA1-deficient Treg.

a, Survival of F^{Cre} x $C1^{+/+ \text{ or } f/f}$ x $Rosa26^{STOP\ f/f\text{-}IKK2ca}$ mice that express one allele of the constitutively active IKK2/β mutant IKK2ca upon expression of $Foxp3^{Cre}$. **b-d**, Frequency of $CD4^+$ and $CD8^+$ Tconv with a $CD44^{hi}$ $CD62L^-$ effector memory phenotype in LNs (b), Frequency of Treg among CD4+ T cells and of eTreg among total Treg in LNs (c), and effector cytokine expression of Tconv upon 8-hour ex vivo stimulation on αCD3/CD28-coated plates (d) in indicated mice. **e-f**, Expression of indicated phospho-proteins by YFP^+ Treg from F^{Cre} x $C1^{+/+}$ or x $C1^{f/f}$ mice at baseline and following 30 min. αCD3/CD28 in vitro stimulation. Grey solid histograms show unstained control cells. Tconv were used as internal controls, and showed nor differences (**not shown**). * = p<0.05, *** = p<0.001, and **** = p<0.0001.

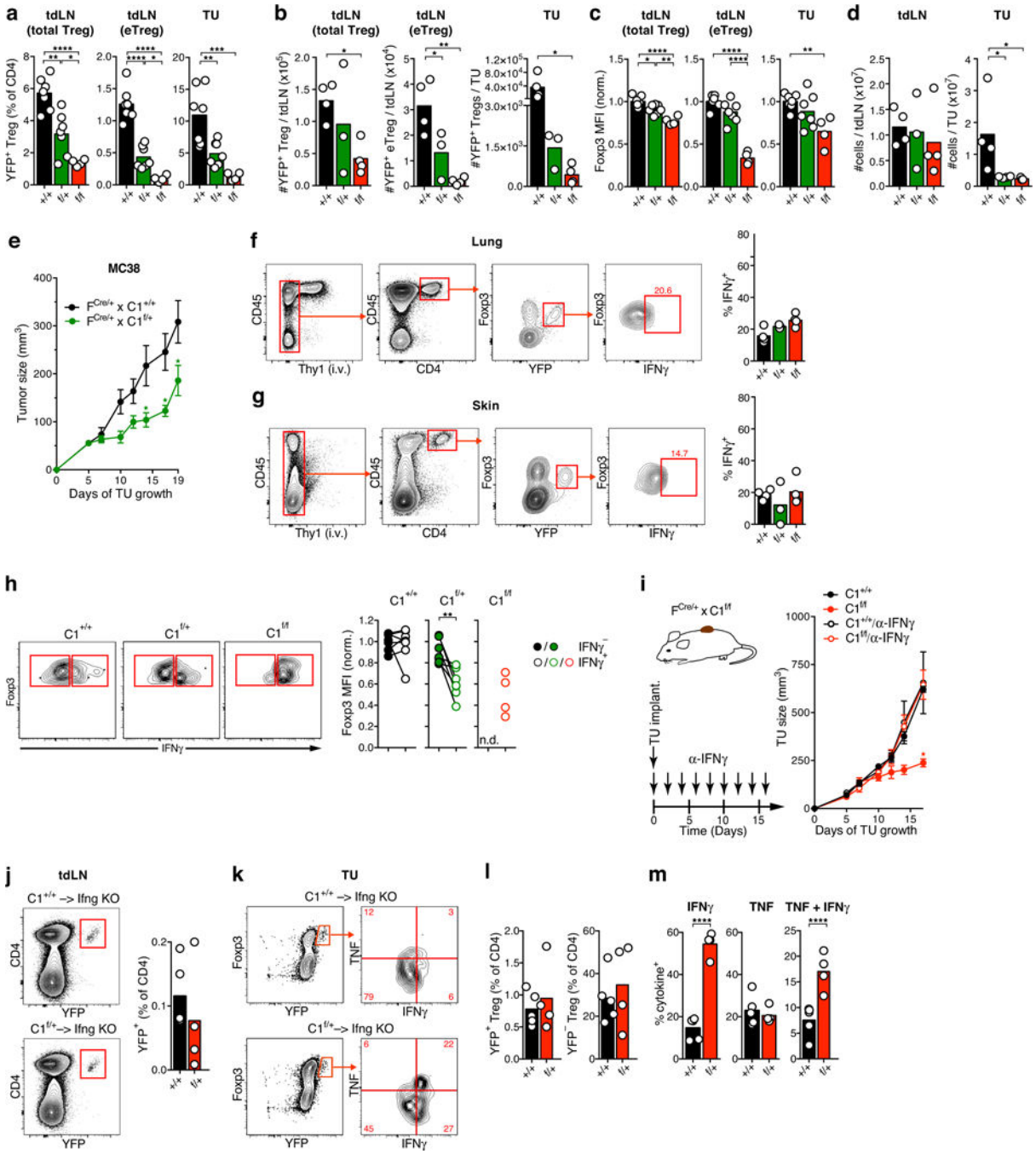

Extended data Figure 8. Role of IFN-γ secretion by Foxp3^{int} unstable Treg selectively in tumor tissue.

a-b, Frequencies of total YFP$^+$ Treg and of YFP$^+$ eTreg among CD4$^+$ T cells (a), absolute YFP$^+$ Treg and eTreg numbers (b), and normalized Foxp3 expression in YFP$^+$ Treg and eTreg (c) in tdLN and tumor tissue of 18 day-old D4M.3A tumors in female heterozygous F$^{Cre/+\ x\ C1+/+,\ f/+,\ f/f}$ mice. **d,** tdLN and tumor cellularities. **e,** Growth of MC38 tumors in in female heterozygous F$^{Cre/+\ x\ C1+/+,\ f/+,\ f/f}$ mice. **f-g**, Tumor-bearing mice were treated with Brefeldin A for 5 hours, i.v. injected with 3 μg of α-Thy1.2 mAbs, and 3 min. later

harvested for direct ex vivo analysis of IFNγ-expression in extravascular YFP$^+$ Treg in lung (f) and skin (g). Gates for IFNγ$^+$ cells drawn based on FMO controls. **h,** Normalized Foxp3 expression in IFNγ$^+$ and IFNγ$^-$ Treg from tumor tissue. n.d. = not detectable. **i,** Tumor growth in indicated mice implanted with D4M.3A melanoma and treated with neutralizing αIFNγ antibody or not. **j,** Frequency of adoptively transferred, YFP$^+$ Treg of indicated genotypes in tdLNs of Ifng KO hosts at day 18 of tumor growth. **k-m**, Frequency (k-l) and effector cytokine expression (m) of adoptively transferred, YFP$^+$ Treg in tumors in Ifng KO hosts. */**/**/**** = $p<0.05/0.01/0.001/0.0001$.

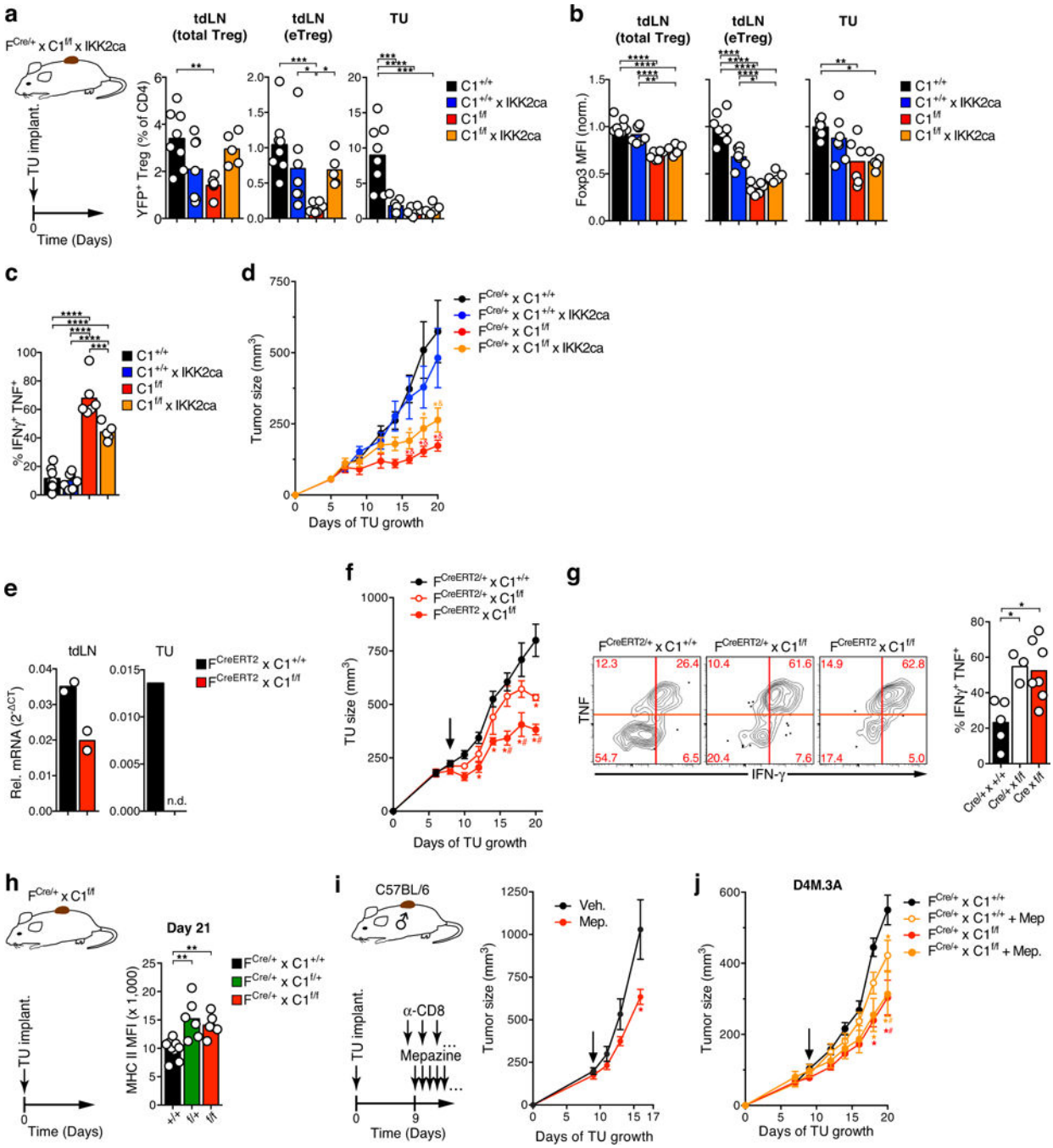

Extended data Figure 9. Restoring NF-κB activation in CARMA1-deficient Treg (cont'd).

a-d, D4M.3A melanoma were implanted into $F^{Cre/+}$ x $C1^{+/+ \text{ or } f/f}$ x $Rosa26^{STOP\ f/f\text{-}IKK2ca}$ mice to record frequencies of YFP^+ Treg and eTreg among $CD4^+$ T cells (a) and their normalized Foxp3 expression (b) in tdLN and tumor tissue, effector cytokine expression by tumor-infiltrating Treg (c), and tumor growth (d). **e**, YFP^+ Treg were sorted from D4M.3A melanoma tissue and tdLN after 5 days of treatment of $Foxp3^{GFP\text{-}CreERT2}$ x $CARMA1^{+/+}$ and x $CARMA1^{f/f}$ mice ('$F^{CreERT2}$ x $C1^{+/+,\ f/f}$') with tamoxifen and analyzed for CARMA1 expression by RT-qPCR. n.d. = not detectable. **f,** Tumor growth in female $F^{CreERT2}$ or

$F^{CreERT2/+}$ x $C1^{+/+, f/f}$ mice, in which CARMA1 was deleted in all ($F^{CreERT2}$) or half ($F^{CreERT2/+}$) of Treg. Arrow indicates tamoxifen treatment start. **g**, In situ-expression in tumor tissue of effector cytokines by YFP^+ Treg 5 days following CARMA1-deletion in half or all Treg. **h,** MHC II expression on tumor-associated macrophages in D4M.3A-implanted $F^{Cre/+}$ x $C1^{+/+, f/+, or f/f}$ mice. **i**, D4M.3A tumor growth in mice treated with depleting αCD8 Ab from day 8 and treated with mepazine or not from day 9. **j**, D4M.3A tumor growth in $F^{Cre/+}$ x $C1^{+/+ or f/f}$ mice treated with Mepazine or vehicle starting on day 9. Graphs show means and individual replicates or ±SEM. */**/**/**** = $p<0.05/0.01/0.001/0.0001$ in a-c, g-i. *,& = any $p<0.05$ vs. $C1^{+/+}$ and $C1^{+/+}$ x IKK2ca, resp. in d. */# = $p<0.05$ vs. $F^{CreERT2}$ x $C1^{+/+}$ / $F^{CreERT2/+}$ x $C1^{f/+}$ in f. */# = any $p<0.05$ vs. $C1^{+/+}$/ $C1^{+/+}$ + Mep. in j.

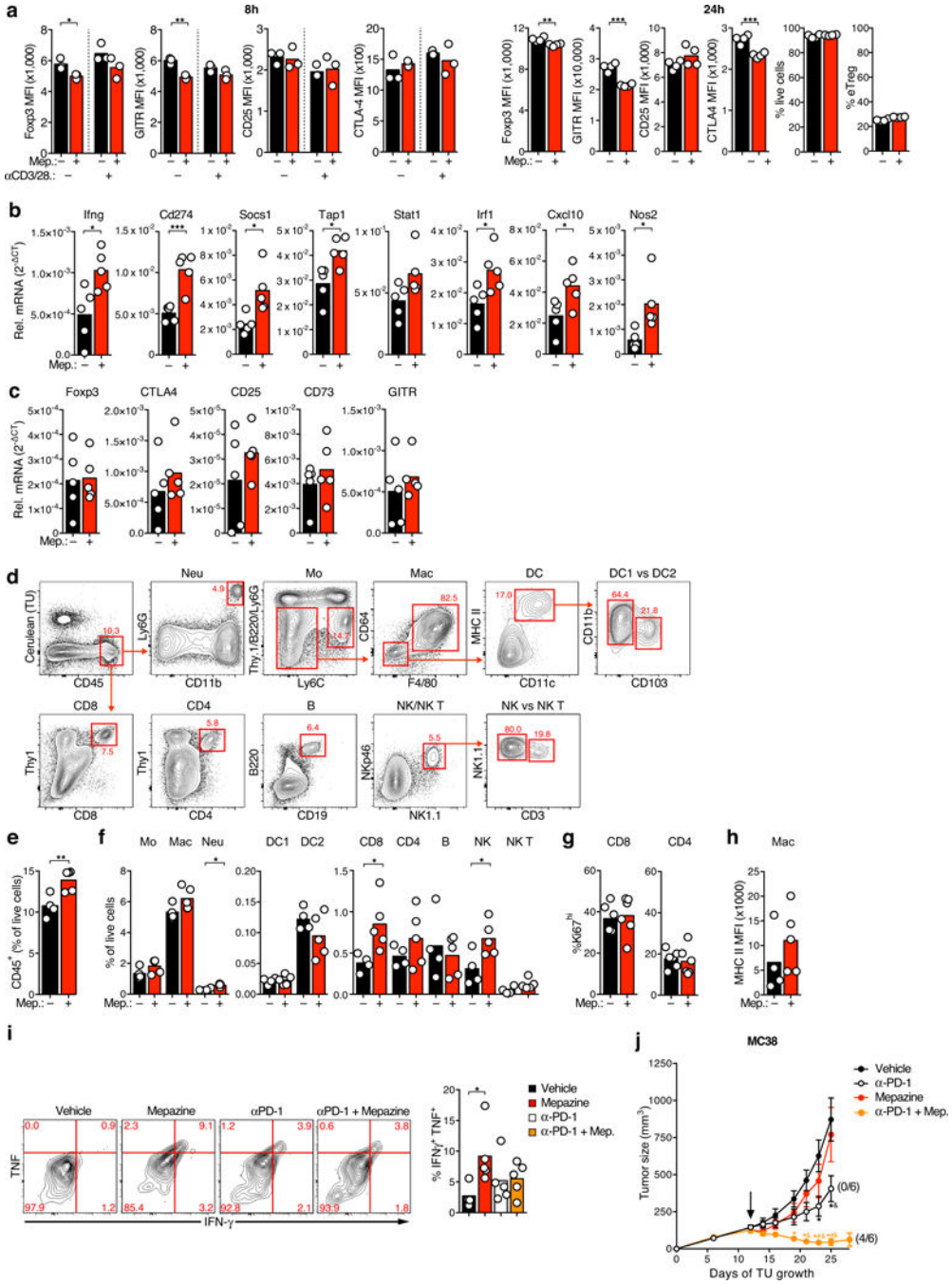

Extended data Figure 10. Mepazine effects on the tumor microenvironment

a, YFP^{+} Treg were sorted from F^{Cre} x C1$^{+/+}$ mice and treated with 10 μM Mepazine or vehicle for 8 or 24 hours with or without concurrent αCD3/28 mAb TCR stimulation (8 h time-point only). Expression of Foxp3, markers of eTreg differentiation, cell viability, and frequency of eTreg were recorded. **b,c** RT-qPCR analysis of expression of *Ifng* and genes of adaptive immune resistance (the PD-L1 gene *Cd274*, *Socs1*), antigen presentation (*Tap1*), IFNγ-signaling (*Stat1, Irf1*), T-cell recruitment (*Cxcl10*), M1 macrophage-activation (*Nos2*) (b) and of Foxp3 and various Treg-associated genes (c) in whole tumor tissue lysate

following 3 days of Mepazine or vehicle treatment. **d-h**, Composition of the tumor tissue immune infiltrate and frequencies of $CD45^+$ cells (e) and of various immune cell subsets (f) as well Ki67 expression by Tconv (g) and MHC II expression by macrophages (h) following 3 days of Mepazine or vehicle treatment. **i**, Effector cytokine co-expression by tumor-infiltrating Treg following 12 days Mepazine and αPD-1 Ab treatment. **j,** Synergistic tumor control of MC38 colon carcinoma through αPD-1 and mepazine combination treatment in female C57BL/6 hosts. Numbers in parentheses indicate fraction of mice without relapse for >12 months following discontinuation of treatment. * = any $p<0.05$ vs. Vehicle, # = $p<0.05$ vs. αPD-1, and & = $p < 0.05$ vs. Mepazine in j. */**/*** = $p<0.05/0.01/0.001$ in other panels.

Supplementary Material

Refer to Web version on PubMed Central for supplementary material.

Acknowledgements.

We thank the MGH Pathology Flow Cytometry Core and Noor Ali-Akbar for technical assistance. This study was funded by an EMBO fellowship (ALTF534-2015) and a Marie Curie Global Fellowship (750973) (M.D.P.), DFG Fellowships (PR 1652/1-1 to J.N.P and US 116/2-1 to S.M.U), NIH T32 CA207021 (V.M.), a Sara Elizabeth O'Brien Fellowship (F.M.), and Melanoma Research Alliance Senior Investigator Award MRA-348693, NIH AI123349, and the Bob and Laura Reynolds MGH Research Scholar Award (T.R.M.).

References

1. Savage PA, Leventhal DS & Malchow S Shaping the repertoire of tumor-infiltrating effector and regulatory T cells. Immunol. Rev 259, 245–258 (2014). [PubMed: 24712470]
2. Mellman I, Coukos G & Dranoff G Cancer immunotherapy comes of age. Nature 480, 480–489 (2011). [PubMed: 22193102]
3. Spranger S et al. Up-regulation of PD-L1, IDO, and T(regs) in the melanoma tumor microenvironment is driven by CD8(+) T cells. Sci Transl Med 5, 200ra116–200ra116 (2013).
4. Bauer CA et al. Dynamic Treg interactions with intratumoral APCs promote local CTL dysfunction. J. Clin. Invest 124, 2425–2440 (2014). [PubMed: 24812664]
5. Meininger I & Krappmann D Lymphocyte signaling and activation by the CARMA1-BCL10-MALT1 signalosome. Biol. Chem 397, 1315–1333 (2016). [PubMed: 27420898]
6. Medoff BD et al. Differential requirement for CARMA1 in agonist-selected T-cell development. Eur. J. Immunol 39, 78–84 (2009). [PubMed: 19130560]
7. Molinero LL et al. CARMA1 Controls an Early Checkpoint in the Thymic Development of FoxP3+ Regulatory T Cells. J. Immunol 182, 6736–6743 (2009). [PubMed: 19454668]
8. Barnes MJ et al. Commitment to the regulatory T cell lineage requires CARMA1 in the thymus but not in the periphery. Plos Biol 7, e51 (2009). [PubMed: 19260764]
9. Brüstle A et al. MALT1 is an intrinsic regulator of regulatory T cells. Cell Death Differ 24, 1214–1223 (2017). [PubMed: 26405015]
10. Schmidt-Supprian M et al. Differential dependence of CD4+CD25+ regulatory and natural killer-like T cells on signals leading to NF-kappaB activation. Proc. Natl. Acad. Sci. U.S.A 101, 4566–4571 (2004). [PubMed: 15070758]
11. Smigiel KS et al. CCR7 provides localized access to IL-2 and defines homeostatically distinct regulatory T cell subsets. J. Exp. Med 211, 121–136 (2014). [PubMed: 24378538]
12. Long M, Park S-G, Strickland I, Hayden MS & Ghosh S Nuclear factor-kappaB modulates regulatory T cell development by directly regulating expression of Foxp3 transcription factor. Immunity 31, 921–931 (2009). [PubMed: 20064449]

13. Vasanthakumar A et al. The TNF Receptor Superfamily-NF-κB Axis Is Critical to Maintain Effector Regulatory T Cells in Lymphoid and Non-lymphoid Tissues. Cell Rep 20, 2906–2920 (2017). [PubMed: 28889989]
14. Messina N et al. The NF-κB transcription factor RelA is required for the tolerogenic function of Foxp3(+) regulatory T cells. J. Autoimmun 70, 52–62 (2016). [PubMed: 27068879]
15. Oh H et al. An NF-κB Transcription-Factor-Dependent Lineage-Specific Transcriptional Program Promotes Regulatory T Cell Identity and Function. Immunity 47, 450–465.e5 (2017). [PubMed: 28889947]
16. Grinberg-Bleyer Y et al. NF-κB c-Rel Is Crucial for the Regulatory T Cell Immune Checkpoint in Cancer. Cell 170, 1096–1108.e13 (2017). [PubMed: 28886380]
17. Yu J et al. Regulation of T-cell activation and migration by the kinase TBK1 during neuroinflammation. Nat Commun 6, 6074 (2015). [PubMed: 25606824]
18. Jenkins MH et al. Multiple murine BRaf(V600E) melanoma cell lines with sensitivity to PLX4032. Pigment Cell Melanoma Res 27, 495–501 (2014). [PubMed: 24460976]
19. Pierson W et al. Antiapoptotic Mcl-1 is critical for the survival and niche-filling capacity of Foxp3^{+} regulatory T cells. Nat. Immunol 14, 959–965 (2013). [PubMed: 23852275]
20. Overacre-Delgoffe AE et al. Interferon-γ Drives Treg Fragility to Promote Anti-tumor Immunity. Cell 169, 1130–1141.e11 (2017). [PubMed: 28552348]
21. Gewies A et al. Uncoupling Malt1 threshold function from paracaspase activity results in destructive autoimmune inflammation. Cell Rep 9, 1292–1305 (2014). [PubMed: 25456129]
22. Jaworski M et al. Malt1 protease inactivation efficiently dampens immune responses but causes spontaneous autoimmunity. EMBO J 33, 2765–2781 (2014). [PubMed: 25319413]
23. Bornancin F et al. Deficiency of MALT1 paracaspase activity results in unbalanced regulatory and effector T and B cell responses leading to multiorgan inflammation. J. Immunol 194, 3723–3734 (2015). [PubMed: 25762782]
24. Nagel D et al. Pharmacologic inhibition of MALT1 protease by phenothiazines as a therapeutic approach for the treatment of aggressive ABC-DLBCL. Cancer Cell 22, 825–837 (2012). [PubMed: 23238017]
25. Schlauderer F et al. Structural analysis of phenothiazine derivatives as allosteric inhibitors of the MALT1 paracaspase. Angew. Chem. Int. Ed. Engl 52, 10384–10387 (2013). [PubMed: 23946259]
26. Fontan L et al. MALT1 small molecule inhibitors specifically suppress ABC-DLBCL in vitro and in vivo. Cancer Cell 22, 812–824 (2012). [PubMed: 23238016]
27. Wang Y et al. MALT1 promotes melanoma progression through JNK/c-Jun signaling. Oncogenesis 6, e365 (2017). [PubMed: 28759024]
28. Thome M, Charton JE, Pelzer C & Hailfinger S Antigen Receptor Signaling to NF- B via CARMA1, BCL10, and MALT1. Cold Spring Harb Perspect Biol 2, a003004–a003004 (2010). [PubMed: 20685844]
29. Le DT et al. PD-1 Blockade in Tumors with Mismatch-Repair Deficiency. N Engl J Med 372, 2509–2520 (2015). [PubMed: 26028255]
30. Rizvi NA et al. Cancer immunology. Mutational landscape determines sensitivity to PD-1 blockade in non-small cell lung cancer. Science (New York, N.Y.) 348, 124–128 (2015).
31. Zaretsky JM et al. Mutations Associated with Acquired Resistance to PD-1 Blockade in Melanoma. N Engl J Med 375, 819–829 (2016). [PubMed: 27433843]
32. Rubtsov YP et al. Regulatory T cell-derived interleukin-10 limits inflammation at environmental interfaces 28, 546–558 (2008).
33. Rubtsov YP et al. Stability of the regulatory T cell lineage in vivo. Science (New York, N.Y.) 329, 1667–1671 (2010).
34. Srinivas S et al. Cre reporter strains produced by targeted insertion of EYFP and ECFP into the ROSA26 locus. BMC Dev. Biol 1, 4 (2001). [PubMed: 11299042]
35. Sasaki Y et al. Canonical NF-kappaB activity, dispensable for B cell development, replaces BAFF-receptor signals and promotes B cell proliferation upon activation. Immunity 24, 729–739 (2006). [PubMed: 16782029]

36. Dalton DK et al. Multiple defects of immune cell function in mice with disrupted interferon-gamma genes. Science (New York, N.Y.) 259, 1739–1742 (1993).

37. Godfrey VL, Wilkinson JE, Rinchik EM & Russell LB Fatal lymphoreticular disease in the scurfy (sf) mouse requires T cells that mature in a sf thymic environment: potential model for thymic education. Proc. Natl. Acad. Sci. U.S.A 88, 5528–5532 (1991). [PubMed: 2062835]

38. Egawa T et al. Requirement for CARMA1 in antigen receptor-induced NF-kappa B activation and lymphocyte proliferation. Curr. Biol 13, 1252–1258 (2003). [PubMed: 12867038]

39. Marangoni F et al. The transcription factor NFAT exhibits signal memory during serial T cell interactions with antigen-presenting cells 38, 237–249 (2013).

40. Spiess PJ, Yang JC & Rosenberg SA In vivo antitumor activity of tumor-infiltrating lymphocytes expanded in recombinant interleukin-2. J. Natl. Cancer Inst 79, 1067–1075 (1987). [PubMed: 3500355]

41. Marangoni F et al. Tumor Tolerance-Promoting Function of Regulatory T Cells Is Optimized by CD28, but Strictly Dependent on Calcineurin. J. Immunol 200, 3647–3661 (2018). [PubMed: 29661826]

42. Dobin A et al. STAR: ultrafast universal RNA-seq aligner. Bioinformatics 29, 15–21 (2013). [PubMed: 23104886]

43. Li B & Dewey CN RSEM: accurate transcript quantification from RNA-Seq data with or without a reference genome. BMC Bioinformatics 12, 323 (2011). [PubMed: 21816040]

44. Ritchie ME et al. limma powers differential expression analyses for RNA-sequencing and microarray studies. Nucleic Acids Res 43, e47 (2015). [PubMed: 25605792]

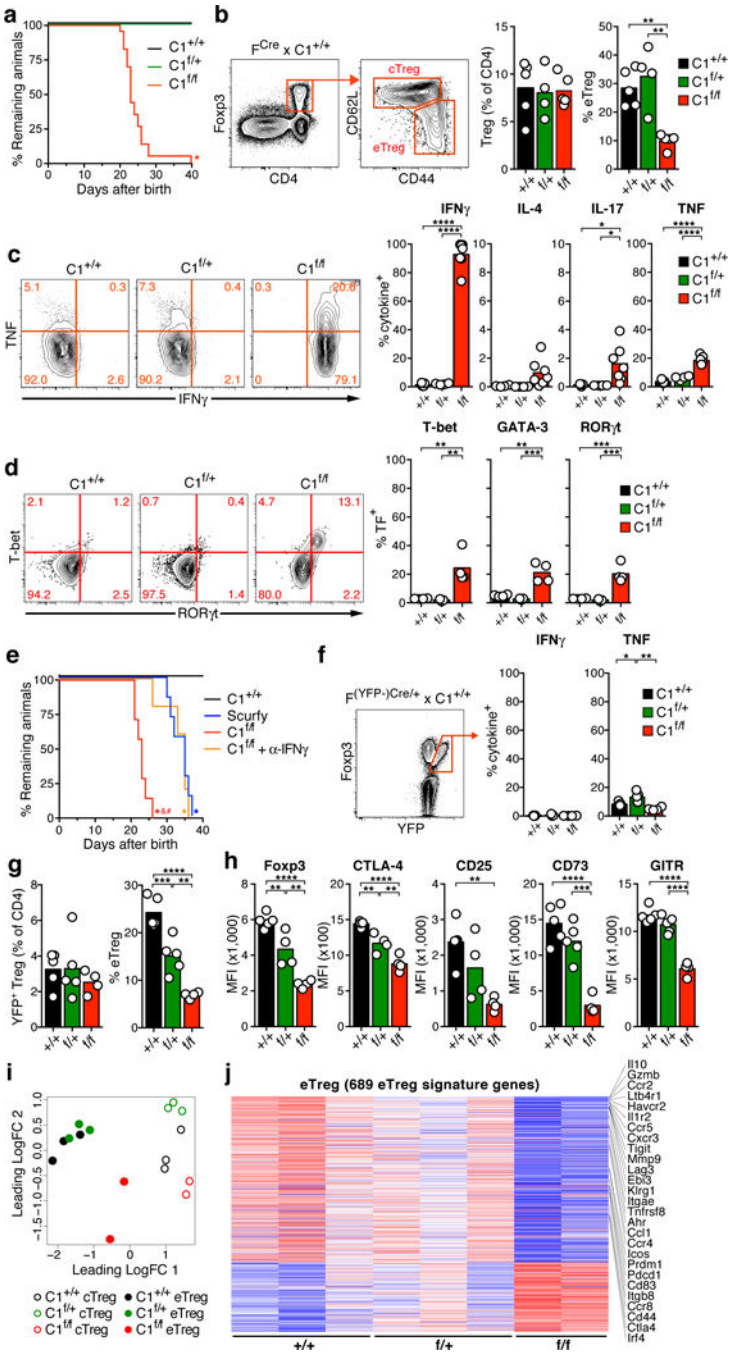

Figure 1. Loss of CARMA1 in Treg is fatal, but reduced expression is sufficient to maintain immune tolerance.

a, survival of F^{Cre} x $C1^{+/+, f/+, f/f}$ mice. (n=8, 10, and 20/group, resp.) **b**, Frequency of Treg among $CD4^+$ T cells and of eTreg among total Treg in LNs. **c-d** Expression of cytokines (c) and transcription factors (d) in LN Treg upon ex vivo-stimulation. **e**, Survival of F^{Cre} x $C^{f/f}$ mice treated with α-IFNγ Abs from day 14 of life, compared to F^{Cre} x $C1^{+/+}$ and *scurfy* mice. **f,** Cytokine expression of YFP^+ Treg from LNs of 9 week-old female heterozygous $F^{Cre/+}$ x $C1^{+/+}$, $C1^{f/+}$, and $C1^{f/f}$ mice upon ex vivo-stimulation. **g,** Frequency of YFP^+ Treg

among $CD4^+$ T cells and of YFP^+ eTreg among total YFP^+ Treg in LNs. **h,** Expression of indicated proteins in YFP^+ eTreg from 9 week-old mice. Data in b-h represent 2 independent experiments with similar results. Graphs show means and either individual replicates or ±SEM. *,&,# = $p<0.05$ vs. WT, *scurfy*, and αIFNγ, respectively in a, e. */**/***/**** = $p<0.05/0.01/0.001/0.0001$ in other panels. **i-j**, Bulk RNA-seq analysis of YFP^+ cTreg and eTreg from LNs of $F^{Cre/+}$ x $C1^{+/+}$, $C1^{f/+}$, and $C1^{f/f}$ mice. Principal component analysis of transcriptomes (i). Scaled expression of 'eTreg signature' genes (j) by eTreg (defined by fold change > 2 and $p_{adj} < 0.01$ between $C1^{+/+}$ cTreg and $C1^{+/+}$ eTreg). Selected eTreg-genes are annotated.

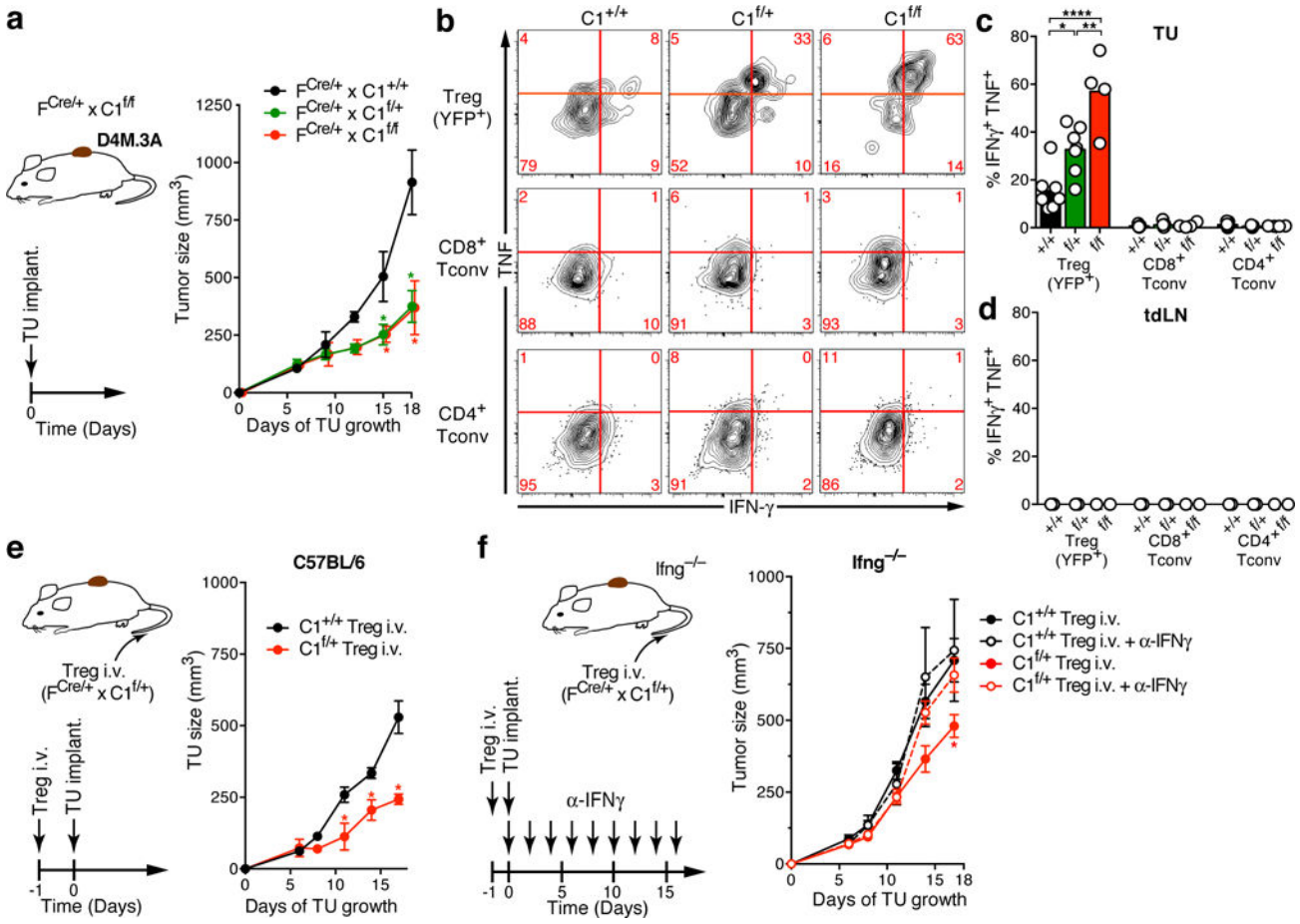

Figure 2. Reduced CARMA1-expression converts tumor-infiltrating Treg into IFNγ-secreting effector cells that dominantly control tumor growth.

a-d, Female Foxp3$^{YFP\text{-}Cre/+}$ x CARMA1$^{+/+}$, CARMA1$^{f/+}$, and CARMA1$^{f/f}$ mice ('F$^{Cre/+}$ x C1$^{+/+,\ f/+,\ f/f}$') were implanted with D4M.3A melanoma, and tumor growth recorded (a). In situ expression in tumor tissue (b-c) or tdLNs (d) of effector cytokines in YFP$^+$ Treg lacking one or both alleles of *Carma1* as well as in CD4$^+$ and CD8$^+$ Tconv 18 days after tumor implantation. **e-f**, 10^6 YFP$^+$ Treg from F$^{YFP\text{-}Cre/+}$ x C1$^{f/+}$ or x C1$^{+/+}$ mice were i.v. injected into either C57BL/6 (e) or IFNγ-deficient (f) hosts, which were implanted with D4M.3A melanoma the following day, and tumor growth recorded. Some IFNγ-deficient hosts were treated with neutralizing α-IFNγ antibody. Data represent 2 independent replicates with similar results. Graphs show means and either individual replicates or ±SEM. * = $p<0.05$ in a, e-f. */**/**** = $p<0.05/0.01/0.0001$ in c-d.

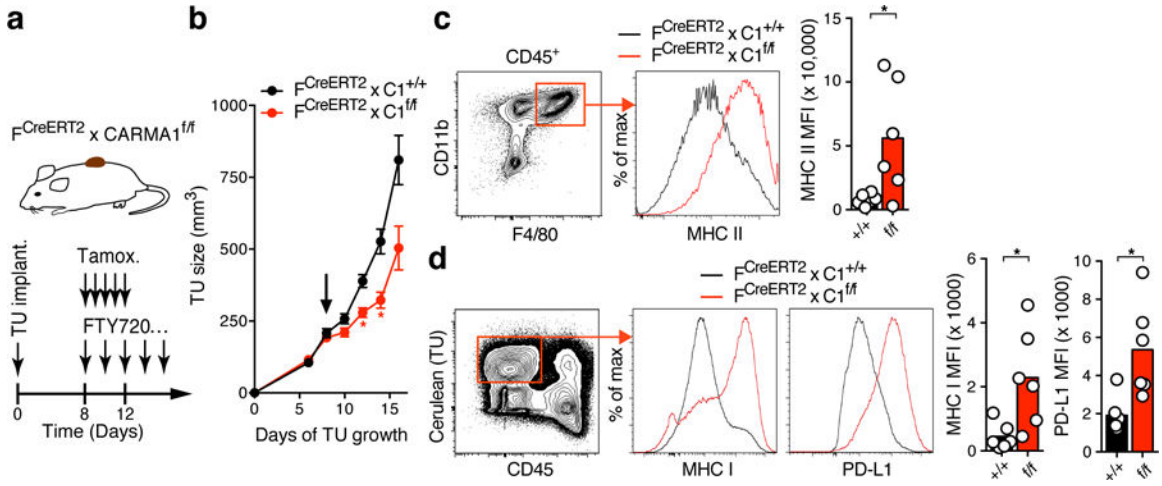

Figure 3. CARMA1-deleted Treg rapidly induce tumor inflammation but also adaptive immune resistance.

a, D4M.3A melanoma growth in Foxp3$^{GFP\text{-}CreERT2}$ x CARMA1$^{+/+}$ and CARMA1$^{f/f}$ mice ('F^{CreERT2} x C1$^{+/+,\ f/f}$') treated with tamoxifen from days 8–12 as well as with FTY720 starting the same day until the end of the experiment. Arrow indicates treatment start. **c-d,** MHC-II surface expression on F4/80^{+} tumor macrophages (c) and MHC-I as well as PD-L1 expression on D4M.3A tumor cells (expressing blue-fluorescent H2B-Ceruelan) (d) 3 days after initiation of tamoxifen treatment. Data represent 2 independent replicates with similar results. Graphs show means and individual replicates or ±SEM. * = p<0.05.

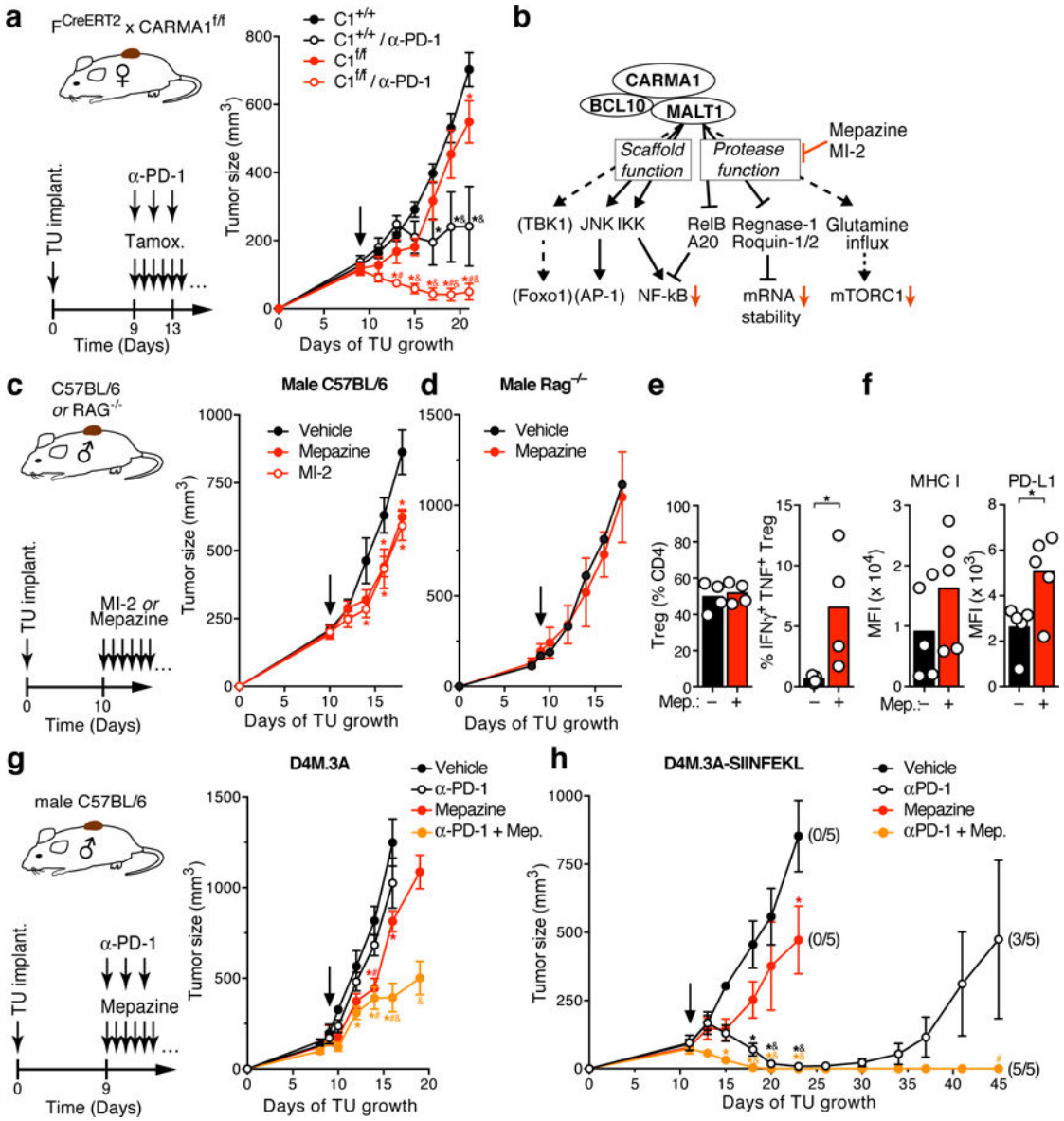

Figure 4. CARMA1-deletion in Treg and pharmacologic MALT1 protease inhibition synergize with αPD-1 ICT.

a, Female Foxp3$^{GFP\text{-}CreERT2}$ x CARMA1$^{+/+}$ and CARMA1$^{f/f}$ mice were implanted with D4M.3A melanoma and starting on day 9 treated with tamoxifen until the end of the experiment as well as with three doses of αPD-1-antibody 29F.1A12 or isotype control, and tumor growth recorded. **b,** CBM-complex effector pathways and predicted effects (red arrows) of MALT1 protease inhibitors mepazine and MI-2. **c-d,** D4M.3A tumor growth in C57BL/6 (c) or RAG1-deficient hosts (d) treated with MALT1 inhibitors. **e-f,** Effects of 3-day Mepazine-treatment on intratumoral Treg frequency and their in situ-effector cytokine-expression (e), MHC-I and PD-L1 expression on tumor cells (f). **g-h,** Synergistic tumor control through αPD-1 and mepazine combination treatment of poorly immunogenic D4M.3A (g) and immunogenic D4M.3A-SIINFEKL (h) tumors in male C57BL/6 hosts. Numbers in parentheses indicate fraction of mice without relapse for >12 months following

discontinuation of treatment. Data in a, c-f represent 2 independent replicates with similar results. Graphs show means and individual replicates or ±SEM. Arrows in graphs indicate treatment start. * = $p<0.05$ vs. $C1^{+/+}$, # = $p<0.05$ vs. $C1^{+/+}$ / αPD-1, and & = $p < 0.05$ vs. $C1^{f/f}$ in a; */#/& = $p<0.05$ vs. Vehicle/αPD-1/Mepazine in g-h, and j; * = $p<0.05$ in e-f.